



# **Première partie**





**ENREGISTREMENTS SÉDIMENTAIRES ET PALÉOMAGNÉTIQUE DU  
QUATERNAIRE SUPÉRIEUR À L'INTÉRIEUR DES ÉVENTAILS  
GLACIOGÉNIQUES DE HOME BAY : DÉFINITION DE L'EXTENSION  
MAXIMALE DE L'INLANDSIS LAURENTIDIEN**

**MÉMOIRE PRÉSENTÉ**

dans le cadre du programme de maîtrise en océanographie  
en vue de l'obtention du grade de maître ès sciences

**PAR**

**©YAN LÉVESQUE**

**Avril 2019**



**Composition du jury :**

**Jean Carlos Montero Serrano, président du jury, Université du Québec à Rimouski**

**Guillaume St-Onge, directeur de recherche, Université du Québec à Rimouski**

**Patrick Lajeunesse, codirecteur de recherche, Université Laval**

**Calvin Campbell, examinateur externe, Commission géologique du Canada**

Dépôt initial le 17 décembre 2018

Dépôt final le 30 mars 2019



## UNIVERSITÉ DU QUÉBEC À RIMOUSKI

Service de la bibliothèque

### Avertissement

La diffusion de ce mémoire ou de cette thèse se fait dans le respect des droits de son auteur, qui a signé le formulaire « *Autorisation de reproduire et de diffuser un rapport, un mémoire ou une thèse* ». En signant ce formulaire, l'auteur concède à l'Université du Québec à Rimouski une licence non exclusive d'utilisation et de publication de la totalité ou d'une partie importante de son travail de recherche pour des fins pédagogiques et non commerciales. Plus précisément, l'auteur autorise l'Université du Québec à Rimouski à reproduire, diffuser, prêter, distribuer ou vendre des copies de son travail de recherche à des fins non commerciales sur quelque support que ce soit, y compris l'Internet. Cette licence et cette autorisation n'entraînent pas une renonciation de la part de l'auteur à ses droits moraux ni à ses droits de propriété intellectuelle. Sauf entente contraire, l'auteur conserve la liberté de diffuser et de commercialiser ou non ce travail dont il possède un exemplaire.



À Sri Aurobindo,

Solvitur ambulando "C'est en  
marchant que la difficulté se  
résout"





## ***REMERCIEMENTS***

Tout d'abord, je souhaite sincèrement remercier mon directeur de recherche, Guillaume St-Onge qui m'a fait confiance dès le début en m'attribuant ce projet de maîtrise, qui m'a guidé tout au long de ce projet et qui a su éclairer ma démarche grâce à ces compétences sur le sujet. Également pour sa compréhension, sa sensibilité, son écoute et son soutien lorsque j'ai eu des problèmes de santé qui ont remis en cause le déroulement de cette maîtrise.

Merci également à mon codirecteur Patrick Lajeunesse pour l'aide précieuse qu'il a apportée en suggérant de nouvelles pistes d'approche et une gamme de possibilités qui a enrichi ce projet de maîtrise. Un remerciement particulier à Pierre-Arnaud Desiagne, Quentin Duboc, Marie-Pier St-Onge et Quentin Beauvais pour le soutien qu'ils m'ont apporté tout au long de ce projet, ainsi que leur disponibilité lorsque j'avais des questions sur des points qui m'étaient particulièrement ambigus. Merci à toute l'équipe de la chaire de recherche en géologie marine qui m'a accompagné durant ces deux années et qui a partagé ma vie de diverses façons.

Enfin, tout cela aurait été difficile sans Omnain, qui m'a accompagnée, aidée, soutenue et encouragée tout au long de la réalisation de ce mémoire. Merci Omy !



## ***RÉSUMÉ***

Le but de cette recherche est d'utiliser les propriétés physiques, magnétiques et sédimentologiques de trois carottes sédimentaires récupérées dans le centre-ouest de la baie de Baffin. Afin de déterminer la chronostratigraphie, les âges radiocarbone de chacune de ces carottes sont combinés avec les résultats paléomagnétiques et les processus sédimentaires en mettant l'accent sur les éventails glaciogéniques (EGs) de Home Bay (carottes AMD16-LGM-09 et AMD0217-01). Les variations millénaires à séculaires de l'orientation du champ magnétique ont été reconstituées puis comparées à des courbes de référence des variations séculaires paléomagnétiques (VSP) provenant de l'Océan Atlantique Nord. Les âges radiocarbone de ces 3 carottes et leurs VSP montrent que celles-ci couvrent une période maximale de 41 000 cal BP. Les enregistrements des variations d'orientation du champ magnétique terrestre calculée à partir de l'analyse en composantes principales respectent les critères de qualité et oscillent autour des valeurs attendues pour la latitude du site selon un modèle dipolaire. Les enregistrements sédimentaires de ces EGs, situés à environ 100 km au large de l'île de Baffin, sont d'un grand intérêt pour la reconstitution des avancées et retraits de l'Inlandsis laurentidien et pour déterminer si ce dernier a atteint la limite du plateau continental au cours de la dernière glaciation. Les données géophysiques combinées aux enregistrements sédimentaires de ces EGs indiquent qu'une série de coulées de débris et de turbidites ont été générées au cours de la dernière glaciation, suggérant ainsi que la marge glaciaire de l'inlandsis s'est étendue jusqu'à cette zone du plateau. Ces résultats nous permettent de proposer une nouvelle délimitation de l'extension maximale de l'Inlandsis laurentidien lors du dernier épisode glaciaire.

Mots clés : [Arctique, baie de Baffin, paléomagnétisme, éventails glaciogéniques, Inlandsis laurentidien, sédiments marins]



## ***ABSTRACT***

The purpose of this research is to use the physical, magnetic and sedimentological properties of three sedimentary cores recovered in west-central Baffin Bay to determine the chronostratigraphic framework (core HU2013-029-077) and sedimentary processes with an emphasis on the Home Bay Trough-Mouth Fans (TMFs) in central-western Baffin Bay (Cores AMD16-LGM-09 and AMD0217-01). In addition, millennial to secular variations in Earth's magnetic field orientation were reconstructed and compared with reference curves of paleomagnetic secular variations (PSV) of the North Atlantic Ocean. The radiocarbon ages from these 3 cores and their PSVs indicate that they cover a maximum period of 41 000 cal BP. The paleomagnetic directional data calculated from the principal component analysis meet the quality criteria and oscillate around the expected values for the site latitude based on a geocentric axial dipole model. The sediment records of these TMFs, located approximately 100 km offshore from Baffin Island, are of great interest in reconstructing the advances and retreats of the Laurentide Ice Sheet (LIS) and determining if it reached the shelf edge during the last glaciation. Geophysical data combined with the sedimentary records of these TMFs indicate that a series of debris flows and turbidites were generated during the last glaciation, suggesting that the ice margin has reached this limit. These results allow us to propose a new delimitation of the maximum extension of the LIS during the Last glacial episode.

Keywords : [Arctic, Baffin Bay, paleomagnetism, trough-mouth fans, Laurentide Ice Sheet, marine sediments]



## ***TABLE DES MATIÈRES***

<b>I</b>	<b>i</b>
REMERCIEMENTS . . . . .	x
RÉSUMÉ . . . . .	xii
ABSTRACT . . . . .	xiv
TABLE DES MATIÈRES . . . . .	xvi
LISTE DES TABLEAUX . . . . .	xviii
LISTE DES FIGURES . . . . .	xix
INTRODUCTION GÉNÉRALE . . . . .	1
Objectif de la recherche . . . . .	2
Organisation du mémoire et contributions . . . . .	3
Présentations officielles lors de congrès . . . . .	3
CHAPITRE 1	
DEFINING THE MAXIMUM EXTENT OF THE LAURENTIDE ICE SHEET IN HOME BAY CROSS-SHELF TROUGH DURING THE LAST GLACIAL EPISODE . . . . .	5
1 Introduction . . . . .	7
2 Regional Setting . . . . .	8
2.1 Hydrography . . . . .	8
2.2 Bedrock Geology . . . . .	11
2.3 Quaternary geology and sedimentation . . . . .	11
3 Material and methods . . . . .	12
3.1 Sediment cores . . . . .	12
3.2 Seismo-stratigraphy and swath bathymetry . . . . .	12
3.3 Physical and geochemical properties . . . . .	13
3.4 Paleomagnetic Analysis . . . . .	14
3.5 Hysteresis Measurements . . . . .	15

3.6	Radiocarbon dating . . . . .	15
4	Results . . . . .	16
4.1	Sea floor morphology and stratigraphic framework . . . . .	16
4.2	Lithofacies . . . . .	27
4.3	Stratigraphy, physical and magnetic properties . . . . .	33
4.4	Magnetic properties . . . . .	39
4.5	Relative Paleointensity (RPI) Determination and Chronostratigraphy .	41
5	Discussion . . . . .	43
5.1	RDL layers: Glaciogenic debris flows (GDFs) and turbidites . . . . .	43
5.2	Late Pleistocene Baffin Bay chronostratigraphy . . . . .	46
5.3	New delimitation of the maximum extension of the LIS in Home Bay during the Last glacial episode . . . . .	49
6	Conclusions . . . . .	49
	CONCLUSION GÉNÉRALE . . . . .	54
	ANNEXE I	
	MATÉRIEL SUPPLÉMENTAIRE . . . . .	58
	CHAPITRE 2	
	RÉFÉRENCES BIBLIOGRAPHIQUES . . . . .	62



## *LISTE DES TABLEAUX*

1	Coordinates and property of the coring sites . . . . .	13
2	Radiocarbon ages from cores HU2013-029-0077, AMD0217-01 PC and AMD 16-LGM-09CASQ. Radiocarbon ages were calibrated ages using the CALIB version 7.1 software (Stuiver and Reimer 1993) and the Marine13 calibration curve (Reimer et al. 2013). Radiocarbon ages from cores HU2013-029-0077 have been taken from Jenner et al., 2018. . . . .	16
3	Sediment facies characteristics of the cores 1Comp and 9CASQ. From left to right: X-radiographs, high-resolution photography, facies, sedimentary structures and processes with the depositional environment. . . . .	28

## ***LISTE DES FIGURES***

- 1 Topographic and bathymetric map of the Baffin Bay area (Jakobsson et al. 2012). The Red star shows the location of the sampling sites from this study: cores HU2013-029-0077 (77PC), AMD0217-01 PC and TWC (1Comp) and AMD 16-LGM-09CASQ (9CASQ). The Yellow star shows the location of core HU2008-029-016PC from Simon et al. (2012). The simplified ocean circulation is represented by the red arrows to illustrate the warm West Greenland current and by the blue arrow to represent the cold Baffin Island current. The white lines represent the ice margin at 16.5 cal ka of the Laurentian Ice Sheet (LIS), Innuitian (IIS) and Greenland (GIS) according to Dyke (2004) and Margold (2015). The red square is a focus of the figure 2. . . . . 9
- 2 Last Glacial Maximum (LGM) extension of the Laurentide Ice Sheet on the continental shelf of western Baffin Bay (Home Bay) during MIS 1 and MIS 2. The dashed black line represents the maximum extension proposed in this study. The solid black line represents the maximum extent according to Dyke (2004). The Red stars represent the sampling sites for cores 77PC, 9CASQ and 1Comp. The red square is a focus on the multibeam image of the Figures 6, 8, 9, 10 and 11. Light grey lines refer to the locations of seismic profiles shown in Figs. 3, 4 and S4. Light grey dashed circle to Fig. 5. See text for details. . . . . 10
- 3 3.5 kHz chirp subbottom profile of core 9CASQ site located at the end of a TMF near the abyssal plain in the lower continental slope of Home Bay. The base of the core contains alternation of rhythmic succession of stratified pebbly mud rich in IRD and probably thin turbidites. The middle contains a turbidite and alternation of mud and IRD layers. The top of the core is composed of postglacial hemipelagic sediments. . . . . 18
- 4 Hunttec profile collected in 1978 showing the thick acoustically stratified interval of core 77PC located on the continental slope of Home Bay. The estimated core depths are indicated with red mark. Figure is modified from Campbell and Bennett (2014). . . . . 19

- 5     3.5 kHz chirp subbottom profile of core AMD0217-01 PC (1Comp) located on the margin of a TMF in the lower continental slope of Home Bay. The base of the core contains a debrite and the top is composed of a layer of postglacial hemipelagic sediments. The orange dashed line delimited a debris flow channel north west of the core and extends to a depth of more than 10 m. This channel is composed of a series of stacked debris flow which accumulate inside this TMF. The estimated core depths (~4m) are indicated with red mark. 20
  
- 6     Multibeam image and morphology of the cross-shelf trough of Home Bay visualized with the QPS Fledermaus software. The bedforms observed within the area contain iceberg scours on the cross shelf and a series of sub-parallel linear gullies going down the slope. The red star corresponds to core 1Comp (AMD0217-01) located in a trough-mouth fans (TMF). . . . . 21
  
- 7     Topographic and bathymetric map of the Baffin Bay area. The white square is an approximate focus on the multibeam image of the figures 6, 8, 9, 10 and 11. See text for details. . . . . 22
  
- 8     Multibeam image and morphology of the cross-shelf trough and submarine gullies within the slope of Home Bay visualized with the QPS Fledermaus software. The bedforms observed within the area contain iceberg scours on the cross-shelf trough and a series of sub-parallel linear gullies going down the slope. The white dashed lines correspond to the limit of 3 TMFs containing cores 9CASQ (AMD16-LGM-09) and 1Comp (AMD0217-01). The black dashed lines represent sediment transport pathways. . . . . 23
  
- 9     Multibeam image of the site of core 1Comp (AMD0217-01) sampled at the edge of a TMF visualized with the QPS Fledermaus software. The white dashed lines represent the delimitation of the TMFs. . . . . 24
  
- 10    Multibeam image obtained as part of the ArcticNet program showing mega-scale glacial lineations (MSGs) and iceberg ploughmarks on the shelf. A series of sub-parallel gullies within the slope of Home Bay are also visible and TMFs on the continental rise at the top of the image. . . . . 25
  
- 11    Multibeam image software showing MSGs associated with the activity of the LIS on the shelf during the last glaciation. MSGs are an unequivocal signature of ice stream activity. They are profiled, subparallel and very elongated lineations which are aligned in the direction of the advances and retreat of the LIS. The black dashed lines represent potential meltwater channels. . . 26

- 12 X-radiographs and high-resolution photography of representative lithofacies from sediment cores of Home Bay TMFs: AMD0217-01 PC and AMD 16-LGM-09CASQ (9CASQ). 1) Massive, matrix-supported diamict facies. Complex diamicton (LF1); 2) Laminated mud rich in IRD (LF2); 3) Silt and sand turbidite (LF3); 4) Laminated mud (LF4); 5) Homogenous mud with IRD (LF5); 6) Carbonate-rich bed with IRD (LF6); 7) Homogenous mud without IRD (LF7). Ticks on the figures represent the depth in cm. See Table 3 for the legend of facies identification and sediment characteristics. N. B. add 30 cm to get the real depths of 1Comp. . . . . 32
- 13 High-resolution physical and magnetic properties of cores 1Comp (A) and 9CASQ (B). See text for details. Significant lithological facies are numbered and highlighted with colors (see also Table 3 and Figure 12 for facies description and depositional environment). The vertical red lines delineate respectively the MAD value of  $5^\circ$  and the expected inclination according to geocentric axial dipole ( $I_{GAD}$ ) at the coring site. . . . . 36
- 14 Grain size signature ( $D_{50}$ ,  $D_{90}$ , sorting) and inclinations of LF3 in core 9CASQ sampled in the lower continental slope of Home Bay. These trends illustrated the normal grading of a turbidite. The orange layer represent the RDL facies. . . . . 38
- 15 . High-resolution physical, geochemical and magnetic properties of cores 77PC (A), 1Comp (B) and 9CASQ (C). See the text for details. Distinct lithological facies are numbered and highlighted with colors. Gray: massive, matrix-supported diamicton facies => Debris flow (LF1); Dark green: Laminated mud rich in IRD (LF2); Orange: silty and sandy turbidites (LF3); Dark brown: Laminated mud (LF4); Pale green: Homogenous mud with IRD (LF5); Beige: detrital carbonate rich in IRD (LF6); Yellow brownish: homogeneous mud without IRD (LF7). See Table 3 for more details on facies identification. . . . . 41
- 16 A. Typical hysteresis curves and derived parameters of cores 77PC, 9CASQ and 1Comp; B: Day plot (Day et al. 1977): RDL= Rapidly deposited layers (turbidite and debrite); C:  $k_{ARM}$  vs.  $k_{LF}$  plot representing estimated magnetic grain size for magnetite (King et al. 1983): Red circle represent RDL and black circles the remaining sediments. . . . . 42
- 17 Schematic model for the main glaciogenic sedimentary processes inside a trough-mouth fan (TMF). . . . . 46

- 18 RPI correlation. Relative paleointensity inter-comparison for the last 45000 cal BP between cores 77PC (this study), 9CASQ (this study), 1Comp (this study) and RPI reference curves from North Atlantic stack (NAPIS-75; Kissel et al. 2000; Laj et al. 2000), Baffin Bay (Core 16PC; Simon et al. 2012) as well as Mediterranean and Somali Stack (Meynadier et al. 1992). Correlative paleointensity features are indicated with dashed black line. RDLs (e.g. debrite and turbidite) are delimited by the grey and blue square. Radiocarbon ages from core HU2013-029-0077 have been taken from (Jenner et al. 2018). 48

## INTRODUCTION GÉNÉRALE

La baie de Baffin est un étroit bassin océanique situé entre l'archipel Arctique canadien et le Groenland. Elle possède une marge continentale étroite le long de l'île de Baffin ainsi qu'un certain nombre de chenaux et de cônes de déjection sous-marins (c.-à-d., éventails glaciogéniques - EGs) répartis sur le talus continental. La baie de Baffin se situe sur l'ancienne marge nord-est de l'Inlandsis laurentidien (IL) et a été le réceptacle des produits de l'érosion glaciaire durant le dernier épisode glaciaire (Brouard and Lajeunesse, 2017; Margold et al., 2015; Stokes, 2017). Une étude à partir des séquences sédimentaires de la baie de Baffin peut donc mettre de l'avant les liens entre la cryosphère, le climat et l'océan afin de mieux comprendre les changements climatiques et environnementaux qui ont lieu dans l'Arctique à cette époque. En effet, les variations paléoclimatiques séculaires à millénaires peuvent être étudiées à l'aide de carottes sédimentaires afin d'identifier les fluctuations des apports sédimentaires associés à la déglaciation et à l'établissement des conditions postglaciaires. Afin de déterminer la stratigraphie et les processus sédimentaires, trois carottes sédimentaires (HU2013-029-077, AMD16-LGM-09 et AMD0217-01) ont été prélevées dans la région de Home Bay à 1220 m, 1076 m et 1153 m de profondeur. Elles font office d'archives des variations géologiques et paléomagnétiques du passé terrestre. Les carottes AMD16-LGM-09 et AMD0217-01 ont été prélevées à l'intérieur d'éventails glaciogéniques dans la région de Home Bay et elles ont été d'un grand intérêt pour la reconstitution des avancées et retraits de l'IL ainsi que pour déterminer si ce dernier a atteint la limite du plateau continental au cours de la dernière glaciation. En effet, pendant les maximums glaciaires, les inlandsis avancent fréquemment jusqu'à la limite du plateau et deviennent la source d'une grande quantité de sédiments qui se déposent au bas de la pente continentale par une série de processus sédimentaires tels les coulées de débris et les courants de turbidité (Dowdeswell et al., 2008; King et al., 1998; Laberg and Vorren, 1995; Taylor et al., 2002; Tripsanas and Piper, 2008). Lorsque ces coulées s'immobilisent, elles peuvent laisser d'importantes couches de dépôts relativement denses et compactés qui s'accumulent à la base du talus continental à l'intérieur

d'éventails glaciogéniques (De Blasio et al., 2004 ; Nygard et al., 2002 ; Vorren and Laberg, 1997). Ceux-ci sont donc les diagnostics de la présence de l'inlandsis sur le plateau continental (Ó Cofaigh et al., 2013). La quasi-absence de carbonate biogénique dans cette région nordique s'est avérée être un défi de taille afin de dater les sédiments. En effet, les matériaux datables tels les foraminifères sont souvent rares, dissous et mal conservés dans les environnements arctiques canadiens, spécialement dans la baie de Baffin (e.g., de Vernal et al., 1992 ; Ledu et al., 2008 ; McKay et al., 2008). Un cadre temporel est néanmoins essentiel afin de déterminer l'âge des coulées de débris et des turbidites retrouvées à l'intérieur des EGs. Une chronostratigraphie des séquences sédimentaires en utilisant une combinaison d'âges radiocarbones et de paléomagnétisme a malgré tout pu être établie. De plus, la géophysique a permis d'identifier des formes et des structures associées aux mouvements de l'IL. En effet, la forte érosion glaciaire sur le plateau continental, ainsi que la morphologie des fonds sous-marins suggèrent une présence de l'inlandsis jusqu'à la limite du plateau continental durant le dernier épisode glaciaire.

## **Objectif de la recherche**

L'objectif principal de cette maîtrise était de déterminer le rôle des fluctuations de l'Inlandsis laurentidien sur les processus sédimentaires dans un système d'éventail glaciogénique (trough-mouth fan) dans la région de Home Bay depuis la dernière glaciation.

Cet objectif a été atteint grâce à la géophysique et aux propriétés physiques et magnétiques des sédiments qui ont permis de déterminer la stratigraphie, la sédimentologie et la morphologie des séquences sédimentaires. Trois carottes sédimentaires qui ont été prélevées au centre-ouest de la baie de Baffin, au large de l'île de Baffin (~100 km), ont permis de déterminer les fluctuations des apports sédimentaires associées à la déglaciation et à l'établissement des conditions postglaciaires. Les points suivants énumèrent les objectifs spécifiques qui ont été atteints pour mener à bien cette étude :

- Reconstituer les variations d'orientation et d'intensité du champ magnétique terrestre afin d'établir la chronostratigraphie des séquences sédimentaires étudiées ;
- Déterminer les processus sédimentaires sur la marge est de l'île de Baffin en utilisant une approche multitraçeurs telle que la géophysique, la distribution granulométrique, la composition chimique et les propriétés magnétiques des sédiments ;
- Identifier les formes et les structures associées aux mouvements de l'Inlandsis laurentidien sur le plateau continental à l'aide de la bathymétrie multifaisceaux.

## **Organisation du mémoire et contributions**

Ce mémoire de maîtrise est rédigé en anglais et est présenté sous la forme d'un article scientifique et sera soumis prochainement à la revue internationale *Boreas* sous la référence :

**Lévesque, Y.,** St-Onge, G., Lajeunesse, P., Desjardins, P.-A., sera soumis prochainement.

Defining the maximum extent of the Laurentide Ice Sheet in Home Bay cross-shelf trough during the Last glacial episode.

## **Présentations officielles lors de congrès**

Durant les deux années de cette maîtrise, j'ai eu la chance de participer à plusieurs congrès à l'échelle nationale et internationale. Selon l'évolution du projet, certains aspects de ma recherche ont été présentés sous forme de présentations orales ou d'affiches. Voici la liste de ces présentations :

**Lévesque, Y.,** St-Onge, G., Lajeunesse, P., 2017. Chronostratigraphie des sédiments du cratère de Corossol, golfe du Saint-Laurent. Affiche lors du congrès du GEOTOP, mars 2017, Forêt Montmorency (Qc), Canada.



**Lévesque, Y., St-Onge, G., Lajeunesse, P., 2017.** Sedimentary changes in Baffin Bay since the last glaciation : the case of the trough mouth fan of Home Bay. Présentation lors du congrès ARCTRAIN, septembre 2017, Bremen (Allemagne).

**Lévesque, Y., St-Onge, G., Lajeunesse, P., 2017.** Sedimentary changes in Baffin Bay since the last glaciation : the case of the Home Bay Trough Mouth Fan. Affiche lors du congrès ARCTIC CHANGE (ArcticNet), décembre 2017, Québec (Qc), Canada.

**Lévesque, Y., St-Onge, G., Lajeunesse, P., 2017.** Enregistrements sédimentaires du Quaternaire Supérieur à l'intérieur des éventails glaciogéniques de Home Bay : une nouvelle détermination de l'étendue maximale de l'inlandsis laurentidien dans la baie de Baffin centrale. Présentation lors du congrès du GEOTOP, mars 2018, Charlevoix (Qc), Canada.

**Lévesque, Y., St-Onge, G., Lajeunesse, P., 2018.** Enregistrements sédimentaires et paléomagnétique du Quaternaire Supérieur à l'intérieur des éventails glaciogéniques de Home Bay. Présentation lors du congrès de l'ACFAS, mai 2018, Chicoutimi (Qc), Canada.

**Lévesque, Y., St-Onge, G., Lajeunesse, P., 2018.** Defining the maximum extent of the Laurentide Ice Sheet in central-eastern Baffin Bay with glaciogenic debris flows and turbidites. Présentation lors du Congrès international de sédimentologie (ISC), août 2018, Québec (Qc), Canada.

## **CHAPITRE 1**

### **DEFINING THE MAXIMUM EXTENT OF THE LAURENTIDE ICE SHEET IN HOME BAY CROSS-SHELF TROUGH DURING THE LAST GLACIAL EPISODE**

Yan Lévesque<sup>1</sup>, Guillaume St-Onge<sup>1</sup>, Patrick Lajeunesse<sup>2</sup> Pierre-Arnaud Desiagne<sup>1</sup>

<sup>1</sup> Institut des sciences de la mer de Rimouski (ISMER), Canada Research Chair in Marine Geology, Université du Québec à Rimouski and GEOTOP

<sup>2</sup> Département de géographie and Centre d'études nordiques, Université Laval

#### **Abstract**

Three sediment cores recovered from Home Bay in central-western Baffin Bay were used to constrain the chronostratigraphy and determine the sedimentary processes of the Home Bay trough-mouth fans (TMFs) and to investigate if the Laurentide Ice Sheet (LIS) reached the shelf edge during the Last Glacial Maximum (LGM). Seven lithofacies were identified in the the cores 1Comp and 9CASQ based on the physical, magnetic and sedimentological properties. Paleomagnetic results from u-channel samples and hysteresis data reveal that the sediments from Home Bay indicate that the sediment recorded a genuine geomagnetic signal that can be used for chronostratigraphic purposes. Geophysical data also allowed the identification of shapes and structures associated with the presence of the LIS on the cross-shelf trough. Mega-scale glacial lineations (MSGL) suggest glacial processes have eroded and molded the shelf during the Quaternary. These landforms are signature of ice stream activity and have probably been used as feeder corridors for TMFs systems. These geomorphological evidences combined with the sedimentary records in the TMFs, radiocarbon ages and paleomagnetism, indicate that a series of debris flows and turbidity currents

were generated during the Last glacial episode, suggesting that the LIS margin reached the shelf edge. These results allow us to propose a new maximum extent of the LIS during the LGM.

# 1 Introduction

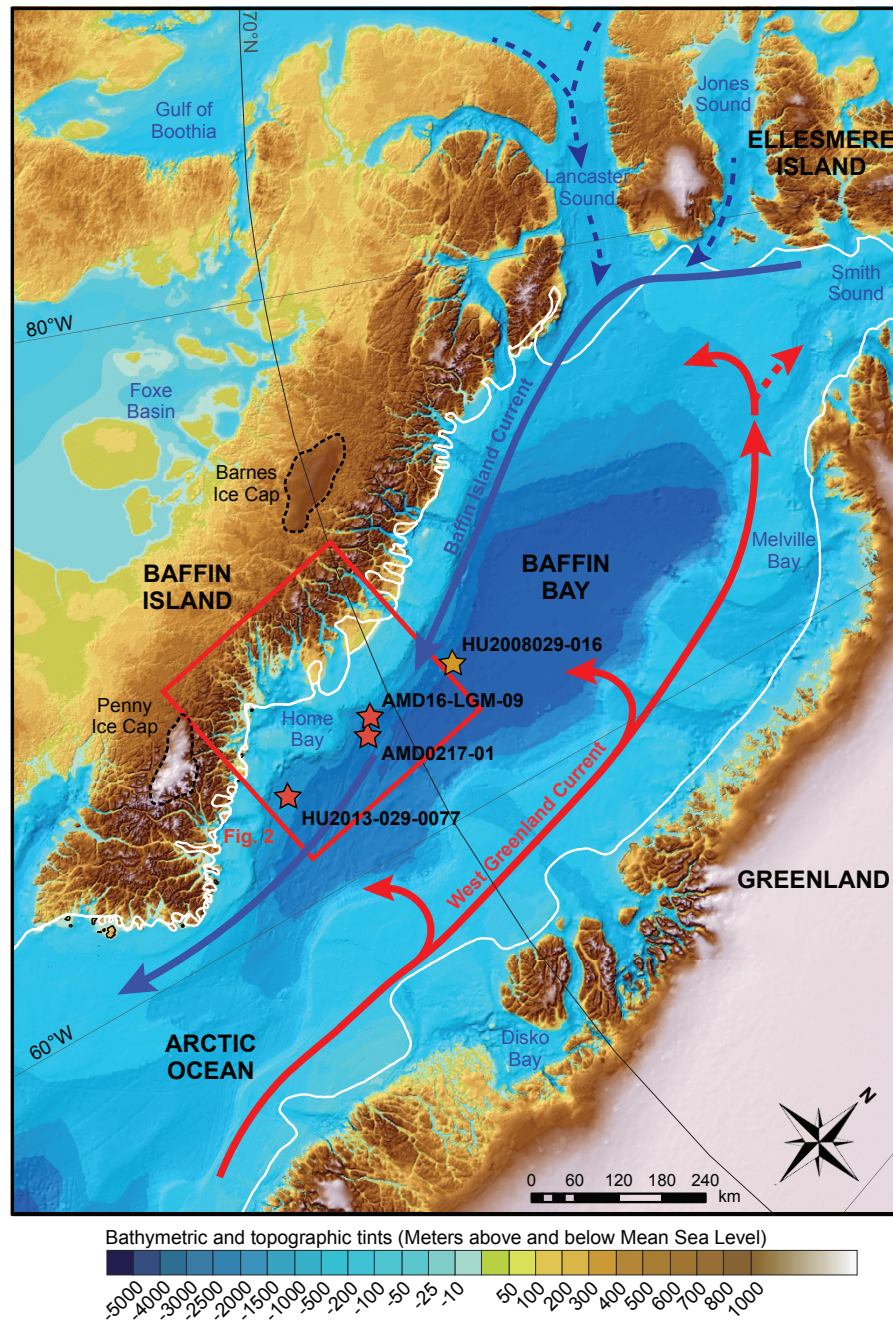
The Laurentide Ice Sheet (LIS) covered most of the of North America during the last glaciation and the Baffin Island margin has been mainly shaped by is successive phases of advance (A. Dyke and Prest 1987). Therefore, being located at the northeast margin of the LIS, Baffin Bay constitutes a unique setting to better understand sedimentary processes related to ice sheet margins (e.g. Margold et al. 2015; Brouard and Lajeunesse 2017; Stokes 2017). During the Last Glacial Maximum (LGM), recent studies have suggested an extensive LIS margin on the Baffin Island shelf, which have reached the shelf edge (Li et al. 2011; Brouard and Lajeunesse 2017; Jenner et al. 2018). Ice sheets generally extends from fjords and small bays across the shelf and extended just beyond the shelf edge (e.g. Andrews 1990; Ó Cofaigh et al. 2013). According to Dyke et al. (2002) and Margold et al. (2015), ice began to recede from its maximum position between 13-12 cal ka BP. Ice sheets near the shelf edge generates change, which result in considerable temporal and spatial variability in the depositional processes of glaciogenic sediments onto the continental slope to ocean basins (Laberg and Vorren 1995; Vorren et al. 1998; King et al. 1998; Nygard et al. 2002). This range of processes are described by many studies including glaciogenic debris flows (GDFs) and turbidity currents, which can extend tens to hundreds of kilometers downslope, being transported by several canyons and gullies and accumulated on submarine deep sea fans (e.g. Ó Cofaigh et al. 2003; De Blasio et al. 2004). These glacial depositional features represent one of the most voluminous downslope remobilizations of glacial sediment progradation, usually described as trough-mouth fans (TMFs); (Laberg and Vorren 1993; King et al. 1998; Nygard et al. 2002; Taylor et al. 2002). They are composed by stacked debrites sometimes switching laterally with turbidites (Laberg and Vorren 1995; Vorren et al. 1998; Tripsanas and Piper 2008). Establishing the temporal evolution setting of this sediment accumulation in a TMF can be highly challenging due to chronostratigraphic limitations. Indeed, datable material such as biogenic carbonates are scarce and/or not well-preserved in Canadian Arctic, including in Baffin Bay (De Vernal et al. 1987; De Vernal et al. 1992; Ledu et al. 2008;

McKay et al. 2008; Simon et al. 2012). In order to circumvent these issues, paleomagnetism combined with radiocarbon dating constitutes a valuable answer to establish the age control of this glaciogenic triggering events (Stoner and St-Onge 2007; St-Onge and Stoner 2011). In fact, sediment cores taken offshore of continental margins at high latitudes are particularly suited for paleoenvironmental high-resolution reconstructions during the Quaternary and can provide continuous and reliable records of geomagnetic field variation (e.g. Andrews and Jennings 1990; Snowball and Sandgren 2002; Snowball and Muscheler 2007; St-Onge et al. 2003; Barletta et al. 2008). In this paper, we present a palaeomagnetic sequence of the relative paleointensity from the continental margin of Baffin Island compared to one paleomagnetic record (Simon et al. 2012) and two other geomagnetic field model (Meynadier et al. 1992; Kissel et al. 2000) in order to obtain a time frame to determine the glaciogenic origin of the debrite and turbidite found in the two sedimentary cores collected within the Home Bay TMFs. In addition, geophysical data allowed the identification of forms and structures associated with the presence of the LIS and/or iceberg drifting offshore on the Home Bay cross-shelf trough.

## **2 Regional Setting**

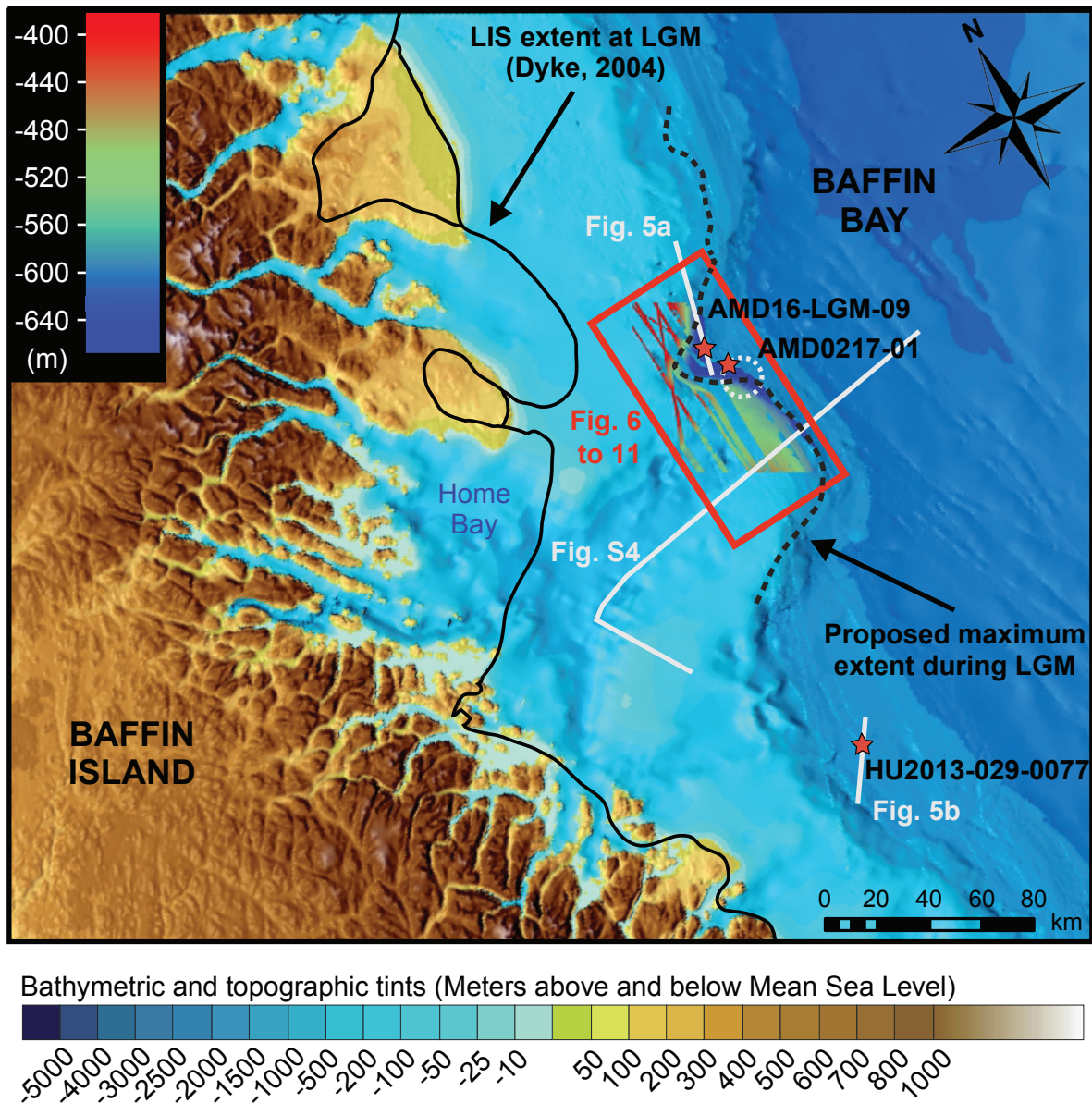
### **2.1 Hydrography**

Baffin Bay is a narrow oceanic basin located between the Canadian Arctic Archipelago and Greenland (Fig. 1). It is about 1300 km long and 450 km wide with a depth of up to 2300 m (Aksu and Piper 1987). It results from the extension of the rift system that opened the shelf of the North Atlantic and Labrador during the Late Cretaceous (McCann 1988; Stanley and Luczaj 2015). An anticlockwise ocean circulation is generated in Baffin Bay and the area is partially covered by sea-ice most of the year, except for August and September (Tang et al. 2004).



**Figure 1:** Topographic and bathymetric map of the Baffin Bay area (Jakobsson et al. 2012). The Red star shows the location of the sampling sites from this study: cores HU2013-029-0077 (77PC), AMD0217-01 PC and TWC (1Comp) and AMD 16-LGM-09CASQ (9CASQ). The Yellow star shows the location of core HU2008-029-016PC from Simon et al. (2012). The simplified ocean circulation is represented by the red arrows to illustrate the warm West Greenland current and by the blue arrow to represent the cold Baffin Island current. The white lines represent the ice margin at 16.5 cal ka of the Laurentian Ice Sheet (LIS), Innuitian (IIS) and Greenland (GIS) according to Dyke (2004) and Margold (2015). The red square is a focus of the figure 2.





**Figure 2:** Last Glacial Maximum (LGM) extension of the Laurentide Ice Sheet on the continental shelf of western Baffin Bay (Home Bay) during MIS 1 and MIS 2. The dashed black line represents the maximum extension proposed in this study. The solid black line represents the maximum extent according to Dyke (2004). The Red stars represent the sampling sites for cores 77PC, 9CASQ and 1Comp. The red square is a focus on the multibeam image of the Figures 6, 8, 9, 10 and 11. Light grey lines refer to the locations of seismic profiles shown in Figs. 3, 4 and S4. Light grey dashed circle to Fig. 5. See text for details.

## **2.2 Bedrock Geology**

The Archaean and Paleoproterozoic cratons form the main units on either side of Baffin Bay. With late Cretaceous rifting continuing throughout the Tertiary, Greenland rifted away from North America forming the Labrador Sea and Baffin Bay and a series of wide grabens (sounds and straits) are observed along the passive margin of the Canadian and Greenland shields (Stein et al. 1979; Hoffman et al. 1989; Scotese and Golonka 1997; Stanley and Luczaj 2015). For this reason, the bay has few Phanerozoic rocks and its geology is mainly characterized by a crystalline basement of Precambrian origin. These old rocks are overlain by a succession of Paleozoic rocks dominated by shallow carbonates such as dolostones and some limestones (Aksu and Piper 1987; Hiscott et al. 1989; Balkwill et al. 1990; Simon et al. 2012; Stanley and Luczaj 2015). The western side of Baffin Bay may also have a significant amount of granitic gneiss and quartzofeldspathic orthogneiss. For this reason, Baffin Island Current (BIC) can transport sediments from this type of rock all along the western side of the island (Harrison et al. 2008).

## **2.3 Quaternary geology and sedimentation**

During the LGM, the Baffin Bay was surrounded by three major ice sheets that flowed into it: the Greenland Ice Sheet (GIS), the Laurentian Ice Sheet (LIS) and the Innuitian Ice Sheet (IIS) (Dyke and Prest 1987; Dyke et al. 2002; Margold et al. 2015; Stokes 2017). The LIS extended across Baffin Island and possibly cover much of its continental shelf, as well as within the Home Bay and a multitude of fjords that incise the islands (Briner et al. 2006; Funder et al. 2011). Deglaciation of the LIS in Baffin Bay began around 16-15 cal ka BP but covered Home Bay area up to 13-12 cal ka BP (Dyke and Prest 1987; Dyke et al. 2002; Dyke 2004; Margold et al. 2015). The sedimentary facies upper Quaternary Baffin Bay succession have been described by several studies that suggested that the LIS may have reached the Baffin Island continental shelf (Aksu and Piper 1987; Hiscott and



Aksu 1994; Praeg et al. 2006; Ó Cofaigh et al. 2013). These facies are mainly controlled by the glacial and interglacial cycles which link the sedimentary processes and resulting sedimentary deposits. When the ice sheets reached the shelf edge, the ice flow triggered a series of sedimentary processes (e.g. turbidity currents and glaciogenic debris flows) that can eventually lead to the formation of TMFs. These TMFs are considered as one of the diagnostics for the presence of ice streams at the shelf edge. In fact, a large part of these TMFs is composed of turbidites and debrites in relation to meltwater processes that periodically incise canyons and submarine valleys (e.g. Tripsanas and Piper 2008; Li et al. 2012). Near the mouths of existing TMFs, basal diamicts are often observed in sediment cores collected on the NE Baffin slope (Table 1 and Fig. 12). They usually represents GDFs that were triggered by glacial advance during the LGM (Jenner et al. 2018).

### **3 Material and methods**

#### **3.1 Sediment cores**

Two piston cores and one large square gravity core (CASQ) were collected with their companion trigger weight cores (TWC) and associated box cores (BC) in central Baffin Bay. Cores AMD16-LGM-09 and AMD0217-01, hereinafter referred as cores 9CASQ and 1Comp, were collected aboard CCGS Amundsen on the Home Bay TMFs, whereas core HU2013-029-0077 (hereinafter referred as 77PC) was collected aboard the CCGS Hudson during cruise 2013029 in order to serve as a chronostratigraphic reference core (Table 1, Fig. 1; Campbell 2014).

#### **3.2 Seismo-stratigraphy and swath bathymetry**

The Home Bay TMF coring sites were determined using a Knudsen 3.5 kHz Chirp subbottom profiler and a Kongsberg Simrad EM-300 (30 kHz) echo-sounders to identify

**Table 1:** Coordinates and property of the coring sites

Core	Latitude (°N)	Longitude (°W)	Location	Water depth (m)	Length (cm)
HU2013-029-0077 PC	68.31	63.79	Slope	1153	597
AMD16-LGM-09 CASQ	68.28	64.56	Slope (TMF)	1220	554
AMD02171-01 PC/TWC	69.24	64.43	Slope (TMF)	1076	350/152
Composite	“	“	“	“	380

areas of Quaternary sedimentary sequences with the presence of mass movements and/or sediment perturbations inside TMFs (Figs. 3 to 11). The high-resolution chirp data were collected with a Knudsen 3.5 kHz subbottom profiling system, integrated and analyzed using the Kingdom Suite software (IHS). The geomorphology of the Home Bay area was examined using high-resolution multibeam bathymetric data that were processed with the CARIS HIPS and SIPS software and visualized with the QPS Fledermaus software. Finally, line 76029\_AG\_280\_1730 (seismic profile) collected in 1976 on board the CCGS Hudson by the Geological Survey of Canada (GSC) has been used to validate if any grounding-zone wedges (GZW) were present in the sector of the Home Bay cross-shelf trough (Fig. S4).

### 3.3 Physical and geochemical properties

In order to define the stratigraphy and sedimentary facies, sections of core 9CASQ were passed through a computerized axial tomography scanner (CAT-Scan) at the Institut national de la recherche scientifique, Centre Eau Terre Environnement (INRS-ETE) in Québec City to characterize the sedimentary facies and sediment structures (St-Onge et al. 2007). Similarly, the sections of core 1Comp were scanned with a GEOTEK XCT digital X-ray system at ISMER. The whole cores were then passed at ISMER on the GEOTEK Multi Sensor Core Logger (MSCL) at 1 cm intervals to measure the low-field volumetric magnetic susceptibility ( $k_{LF}$ ) and the wet bulk density by gamma-ray attenuation, then split, described and photographed. Diffuse spectral reflectance was then acquired with an online Minolta CM-2600d spectrophotometer at 0.5 cm intervals, while the concentration of minor and major

chemical elements (calcium (Ca), strontium (Sr), iron (Fe), Rubidium (Rb), among others) were determined by X-ray fluorescence (XRF) spectrometry at the same intervals using an Olympus Innov-X Handheld XRF analyser Delta Family integrated to the MSCL. The grain size analysis was performed on bulk sediment samples at ISMER using a Beckman Coulter™ LS13320 laser diffraction grain size analyzer at 10 cm intervals, as well as at a higher resolution in specific facies such as in turbidites. Prior to analysis, samples were sieved at 2 mm. A part for a few intervals with a few pebbles, no material larger than 2 mm were recovered.

### **3.4 Paleomagnetic Analysis**

Paleomagnetic data were measured at 1 cm intervals on u-channel samples (2 cm x 2 cm x 150 cm) using a 2G Enterprises™ cryogenic magnetometer at ISMER for chronostratigraphic purposes and to identify possible rapidly deposited layers such as turbidites and debrites that are characterized by low quality paleomagnetic data and shallow inclinations (e.g. St-Onge et al., 2004; Tanty et al., 2016). The measurements performed were: the natural remanent magnetization (NRM), anhysteretic remanent magnetization (ARM), isothermal remanent magnetization (IRM) and the saturation isothermal magnetization (SIRM). Due to the finite spatial resolution of the pick-up coils that integrates measurements over ~7-8 cm (Philippe et al., n.d.), some smoothing occurs. To eliminate the edge effect associated with this response function, the data from the first and last 4 cm of each u-channel were excluded. The NRM was measured and then progressively demagnetized using stepwise alternating field demagnetization (AF) at peak fields from 0 to 75 mT at 5 mT increments. Directions (inclination and declination) of the characteristic remanent magnetization (ChRM) were calculated using the Excel spreadsheet developed by Mazaud (2005) with AF demagnetization steps from 10 to 60 mT (11 steps) for the three cores. This method also provides the maximum angular deviation (MAD) values which are indicative of high-quality directional data when the MAD is lower than 5° for Quaternary paleomagnetic studies (Stoner and St-Onge, 2007). With this spreadsheet, the median destructive field (MDF) of the NRM is also calcu-

lated. It represents the required demagnetization field necessary to reduce the initial magnetic remanence by half of its initial intensity. The MDF is an indicator of magnetic mineralogy reflecting the mean coercivity state of the magnetic grain assemblage and depends on both the grain size and mineralogy (e.g. Stoner and St-Onge 2007; Barletta et al. 2010). The ARM was then induced using a 100 mT AF with a 0.05 mT direct current (DC) biasing field. The ARM was then demagnetized and measured from 0 to 75 mT at every 5 mT. Two IRMs were imparted with a DC field of 0.3 T (IRM) and 0.95 T (SIRM) using a 2G Enterprises pulse magnetizer. Each IRM was measured from 0 to 75 mT at 5 mT demagnetization step increments, while for the SIRM, the steps used were 0, 10, 30, 50 and 70 mT.

### **3.5 Hysteresis Measurements**

In order to define the magnetic mineralogy, hysteresis measurements were performed on the three cores on a small quantity of sediment at 10 cm intervals using a Princeton Measurement Corporation MicroMag 2900 alternating gradient force magnetometer (AGM). The saturation magnetization ( $M_s$ ), the coercive force ( $H_c$ ), the saturation remanence ( $M_{rs}$ ) and the coercivity of remanence ( $H_{cr}$ ) were extracted from the hysteresis data to characterize the magnetic mineralogy and grain size (Day et al. 1977).

### **3.6 Radiocarbon dating**

In order to develop the chronology of the cores,  $^{14}\text{C}$  ages were obtained by accelerator mass spectrometry (AMS) on six samples from mixed planktonic and benthic foraminifera and pachyderma shell (Table 2) at the Laboratoire des sciences du climat et de l'environnement (LSCE), Gif-sur-Yvette, France (cores 9CASQ and 1Comp,) and from Jenner et al. 2018 for the  $^{14}\text{C}$  ages of core 77PC. The conventional ages were then calibrated using the CALIB 7.1 online calibration software (Stuiver and Reimer, 1993) and Marine13 dataset (Reimer et al., 2013) using 1 sigma and a regional reservoir correction  $\Delta R$  of  $220 \pm 20$  years (Coulthard et

**Table 2:** Radiocarbon ages from cores HU2013-029-0077, AMD0217-01 PC and AMD 16-LGM-09CASQ. Radiocarbon ages were calibrated ages using the CALIB version 7.1 software (Stuiver and Reimer 1993) and the Marine13 calibration curve (Reimer et al. 2013). Radiocarbon ages from cores HU2013-029-0077 have been taken from Jenner et al., 2018.

Core	Depth (cm)	Material	Conventional age	Calibrated age (cal. ka BP)	Lab. number
77PC	142	Foraminifers (benthic)	10550 +/- 40	11327	OS-117723
	205	Foraminifers (planktics)	12750 +/- 55	14013	OS-118359
	644 (core catcher)	Pachyderma (Nps)	37900 +/- 1600	41461	OS- UCIAMS 181265
9CASQ	465	Foraminifers (mixed)	35160 +/- 760	39024	ECHo 2458
01-PC	109 (not valid)	Foraminifers (mixed)	10180 +/- 1490	11029	ECHo 2559
	135	Foraminifers (mixed)	12820 +/- 60	14088	ECHo 2558

al., 2010). Of the 6 samples that were analyzed, the results of sample ECHo 2559 could not be validated as only 1  $\mu\text{g}$  of carbon was detected, the current was very low with 0.3  $\mu\text{A}$  and the analysis time was only 2 minutes. This age is therefore only given as an indication.

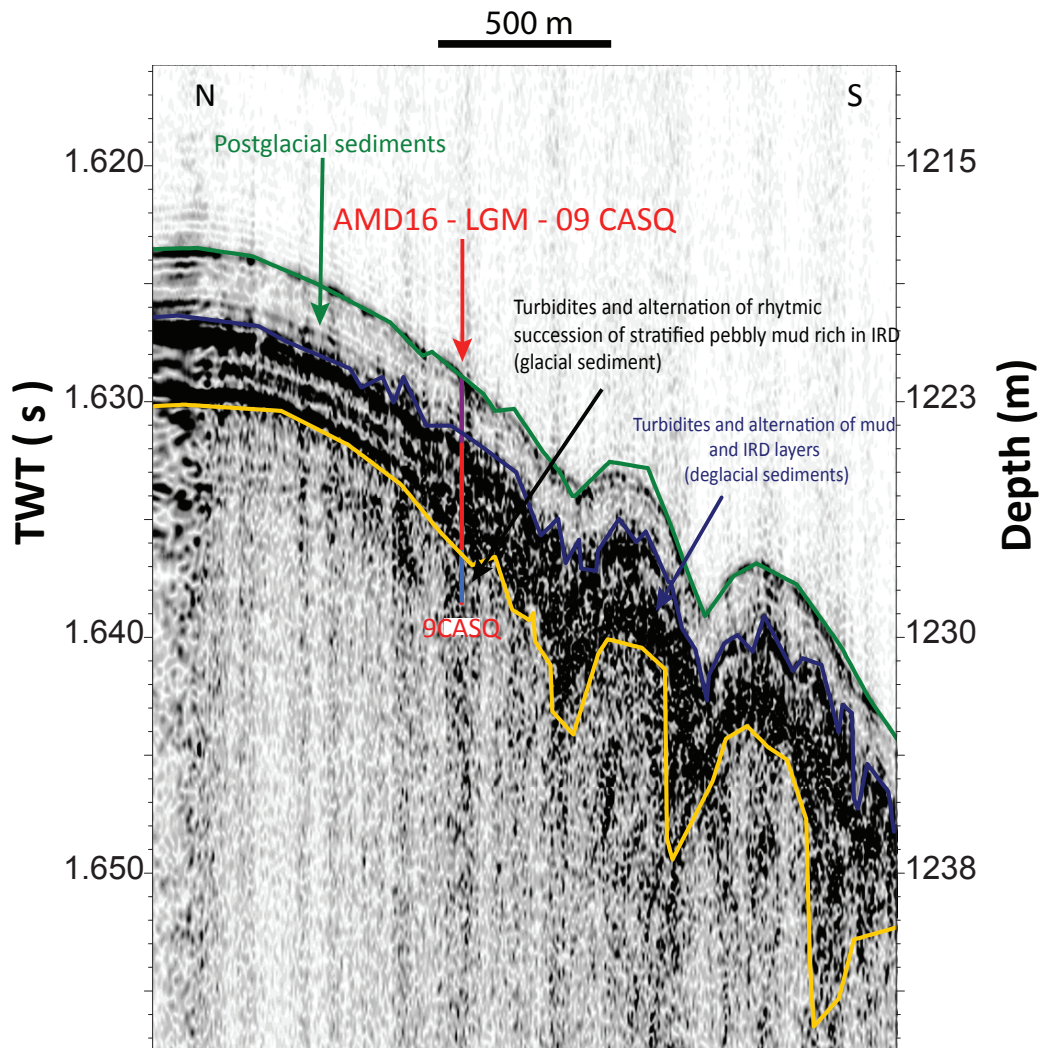
## 4 Results

### 4.1 Sea floor morphology and stratigraphic framework

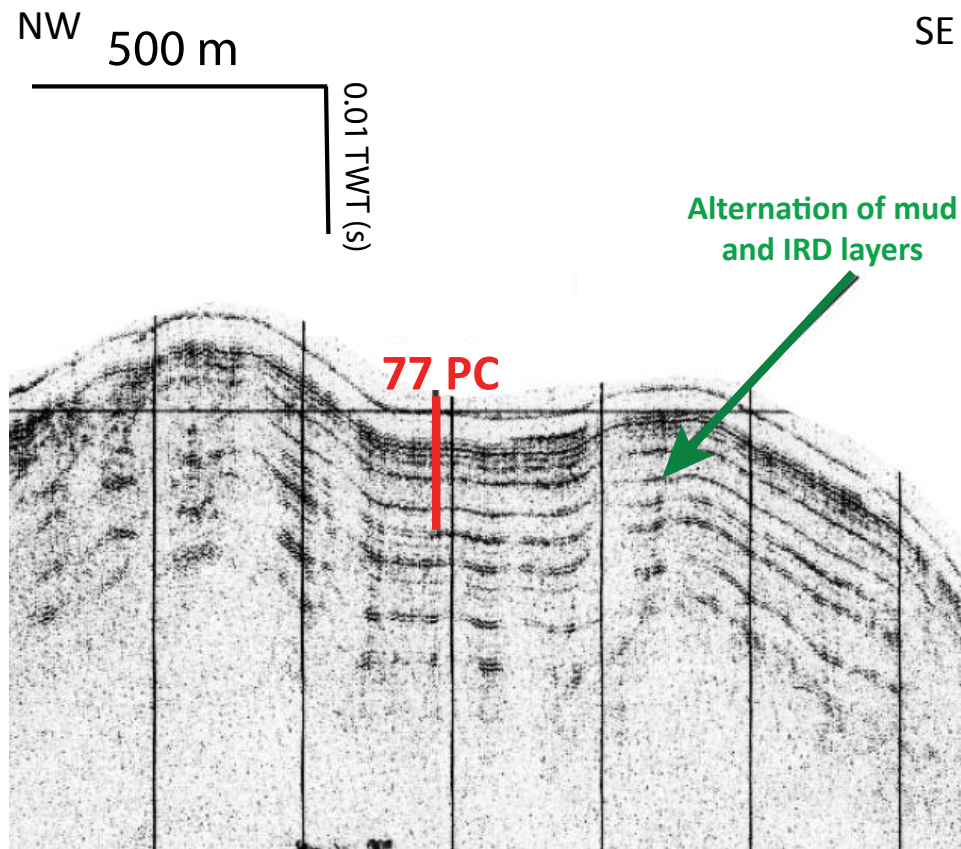
#### 4.1.1 Subbottom profiles

The acoustic subbottom profiles (3.5 kHz) from the sampling location of core 9CASQ show high amplitude parallel acoustic reflections in the middle of the core (362 to 340 cm) where a turbidite and an alternation of rhythmic succession of stratified pebbly mud rich in IRD are observed. This unit is topped by an acoustically transparent unit associated with the postglacial hemipelagic sediments (Fig. 3). The seismic profile of core 77PC is modified from Campbell and Bennett (2014) and is characterized by high amplitude parallel reflections in the basal part of the core as well as transparent acoustic facies associated with the

hemipelagic sediments in the upper part of the core (Fig. 4; Campbell and Bennett, 2014). For core 1Comp, the sequence is characterized by a high amplitude reflection that can be associated with the debrite observed at the base of the core, whereas the uppermost acoustically transparent unit is interpreted as postglacial hemipelagic sediments (Fig. 5). Finally, the available data, including the airgun profile (Fig. S4), do not show any grounding-zone wedge (GZW) in the sector.

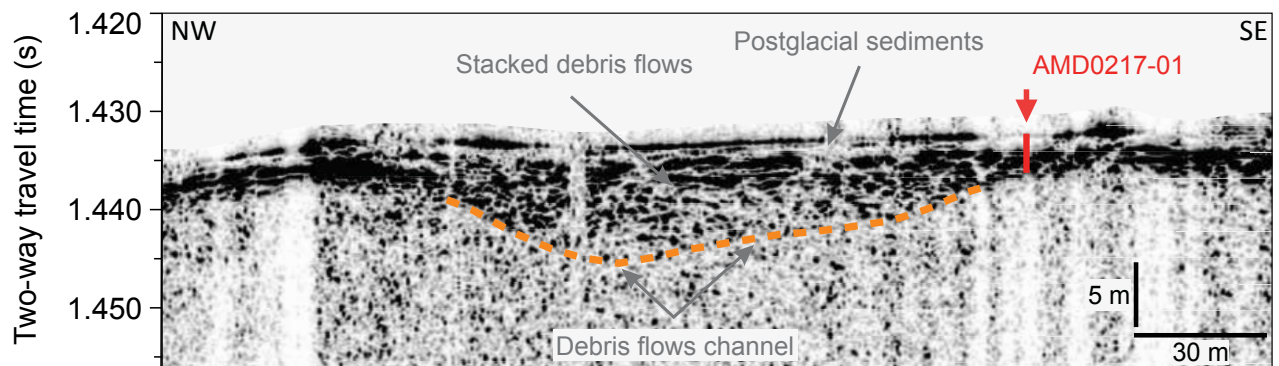


**Figure 3:** 3.5 kHz chirp subbottom profile of core 9CASQ site located at the end of a TMF near the abyssal plain in the lower continental slope of Home Bay. The base of the core contains alternation of rhythmic succession of stratified pebbly mud rich in IRD and probably thin turbidites. The middle contains a turbidite and alternation of mud and IRD layers. The top of the core is composed of postglacial hemipelagic sediments.



**Figure 4:** Hunttec profile collected in 1978 showing the thick acoustically stratified interval of core 77PC located on the continental slope of Home Bay. The estimated core depths are indicated with red mark. Figure is modified from Campbell and Bennett (2014).



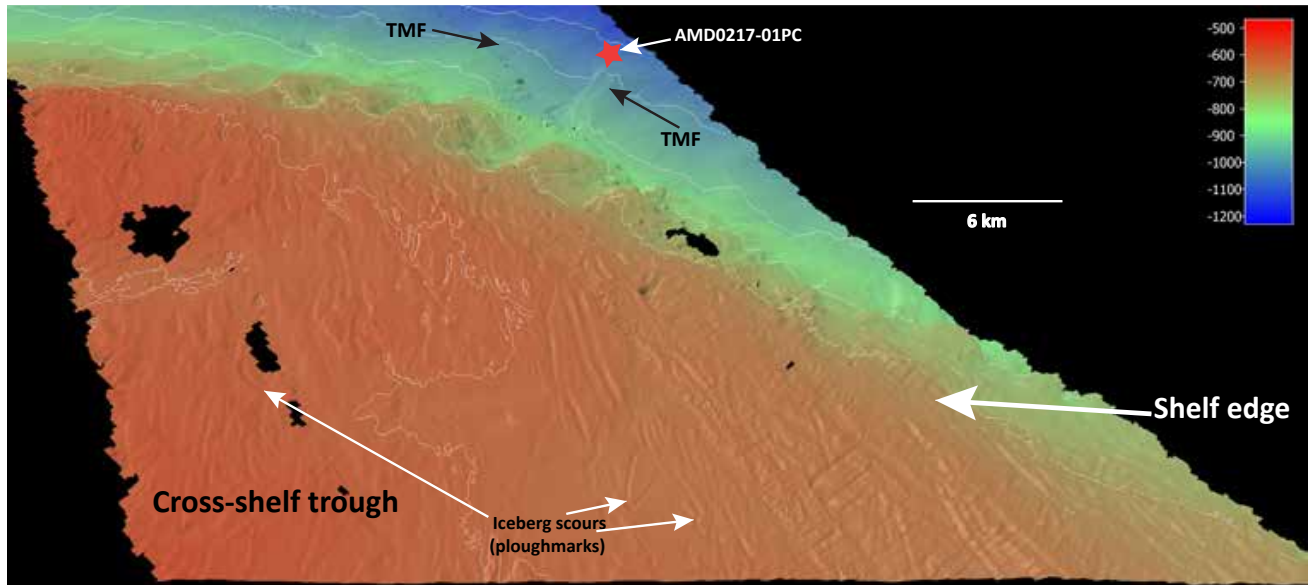


**Figure 5:** 3.5 kHz chirp subbottom profile of core AMD0217-01 PC (1Comp) located on the margin of a TMF in the lower continental slope of Home Bay. The base of the core contains a debrite and the top is composed of a layer of postglacial hemipelagic sediments. The orange dashed line delimited a debris flow channel north west of the core and extends to a depth of more than 10 m. This channel is composed of a series of stacked debris flow which accumulate inside this TMF. The estimated core depths (~4m) are indicated with red mark.

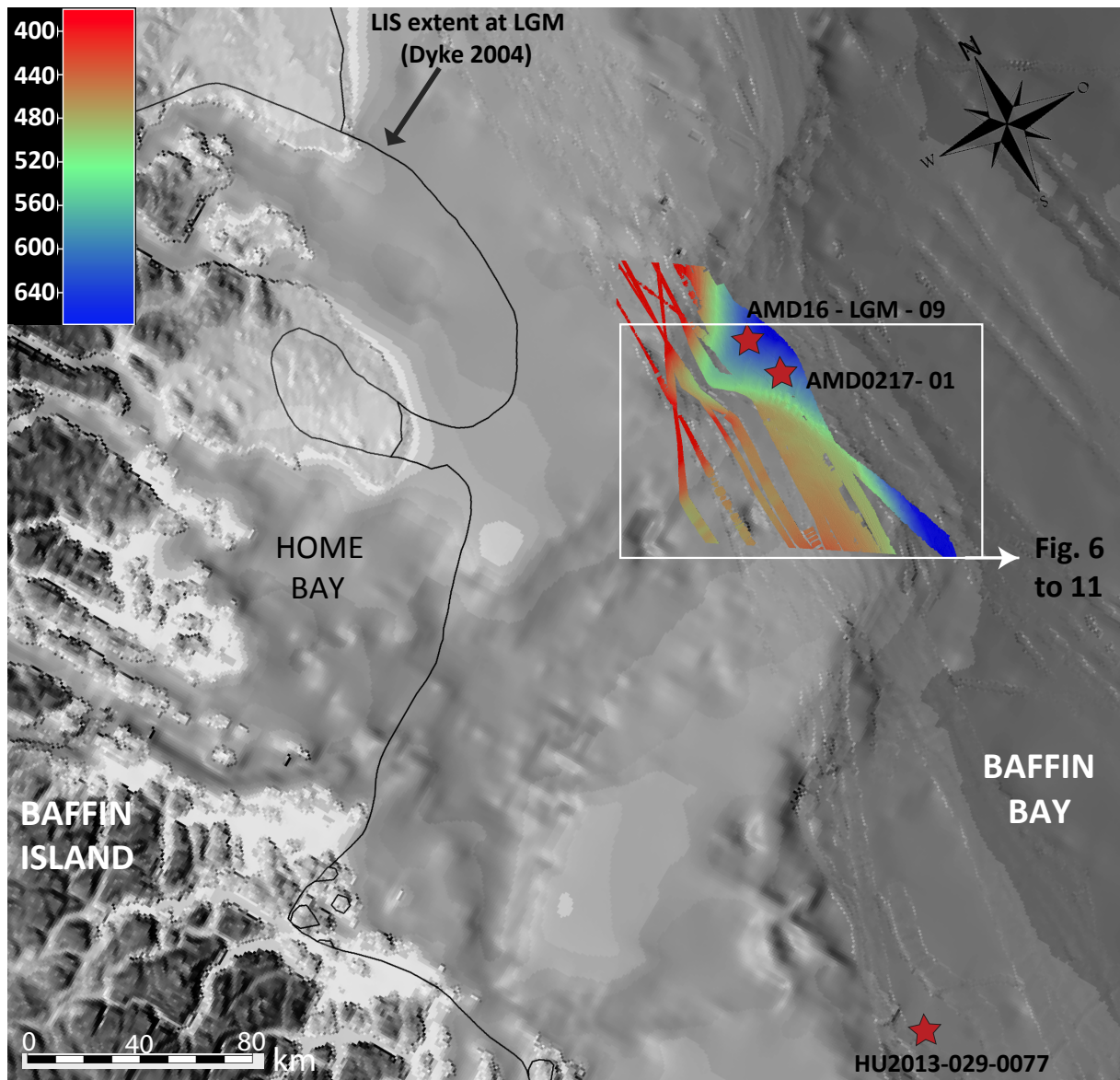
#### 4.1.2 Swath bathymetry

The high-resolution swath bathymetry imagery allowed the identification of shapes and structures associated with the presence of the LIS and/or iceberg drifting offshore. Indeed, the tails of icebergs that drift north to south within the BIC form vast curvilinear and irregular depressions a few meters deep. They sometimes have features showing U or V-shaped forms but can also be very long and almost linear over a distance of more than 20 km and a depth of about 10 m (Figs. 6, 8 and 10).

Another surface of erosion found on the continental shelf are the mega-scale glacial lineation (MSGSL; Dowdeswell et al. 2016; Montelli et al. 2017). These are profiled, subparallel and very elongated lineation which aligns in the direction of the advances and retreat of the LIS in Home Bay. When the ice sheet grows or decay, it has formed wide and deep channel that can reach a depth of some ten of meters (about 40 m in figure 11) and a length of several

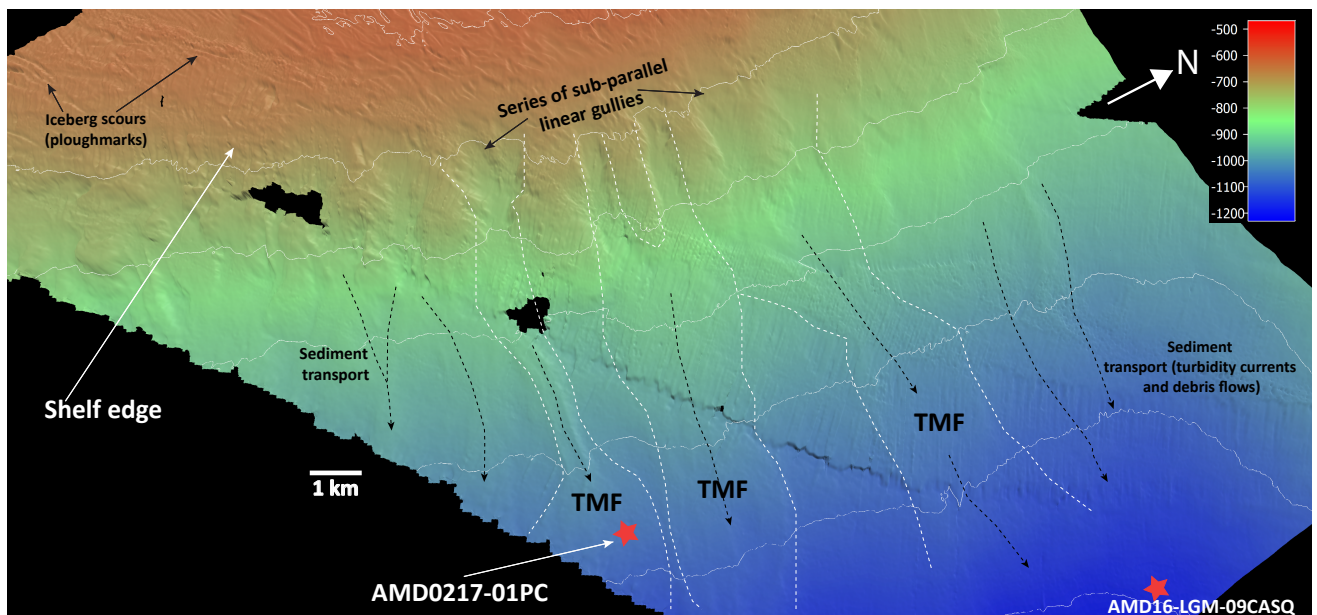


**Figure 6:** Multibeam image and morphology of the cross-shelf trough of Home Bay visualized with the QPS Fledermaus software. The bedforms observed within the area contain iceberg scours on the cross shelf and a series of sub-parallel linear gullies going down the slope. The red star corresponds to core 1Comp (AMD0217-01) located in a trough-mouth fans (TMF).



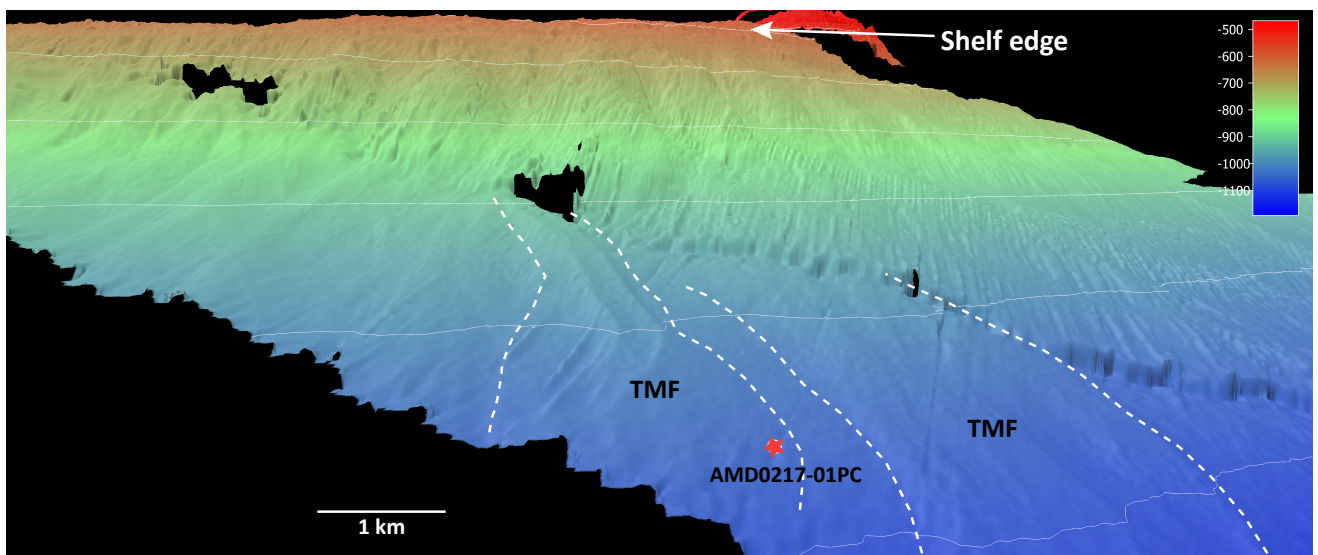
**Figure 7:** Topographic and bathymetric map of the Baffin Bay area. The white square is an approximate focus on the multibeam image of the figures 6, 8, 9, 10 and 11. See text for details.

tens of km (Figs. 10 and 11).

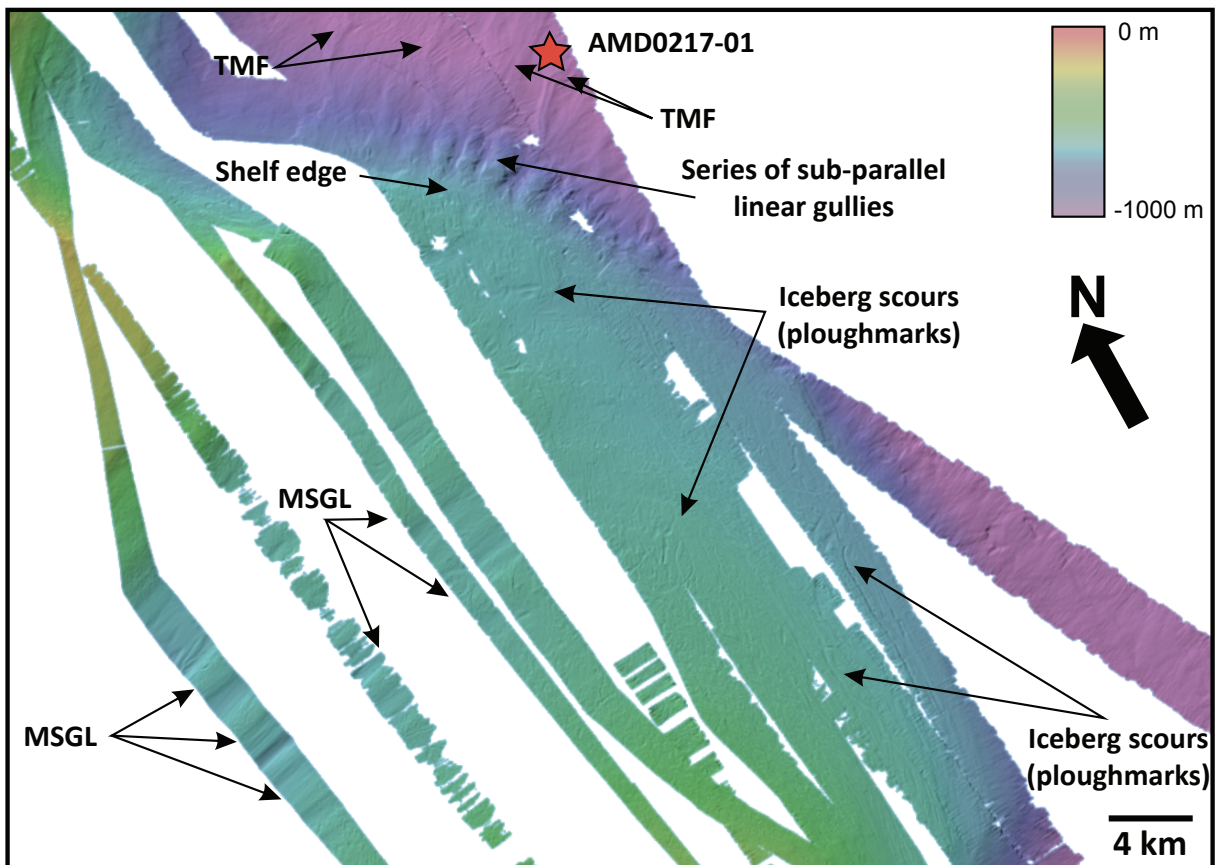


**Figure 8:** Multibeam image and morphology of the cross-shelf trough and submarine gullies within the slope of Home Bay visualized with the QPS Fledermaus software. The bedforms observed within the area contain iceberg scours on the cross-shelf trough and a series of sub-parallel linear gullies going down the slope. The white dashed lines correspond to the limit of 3 TMFs containing cores 9CASQ (AMD16-LGM-09) and 1Comp (AMD0217-01). The black dashed lines represent sediment transport pathways.

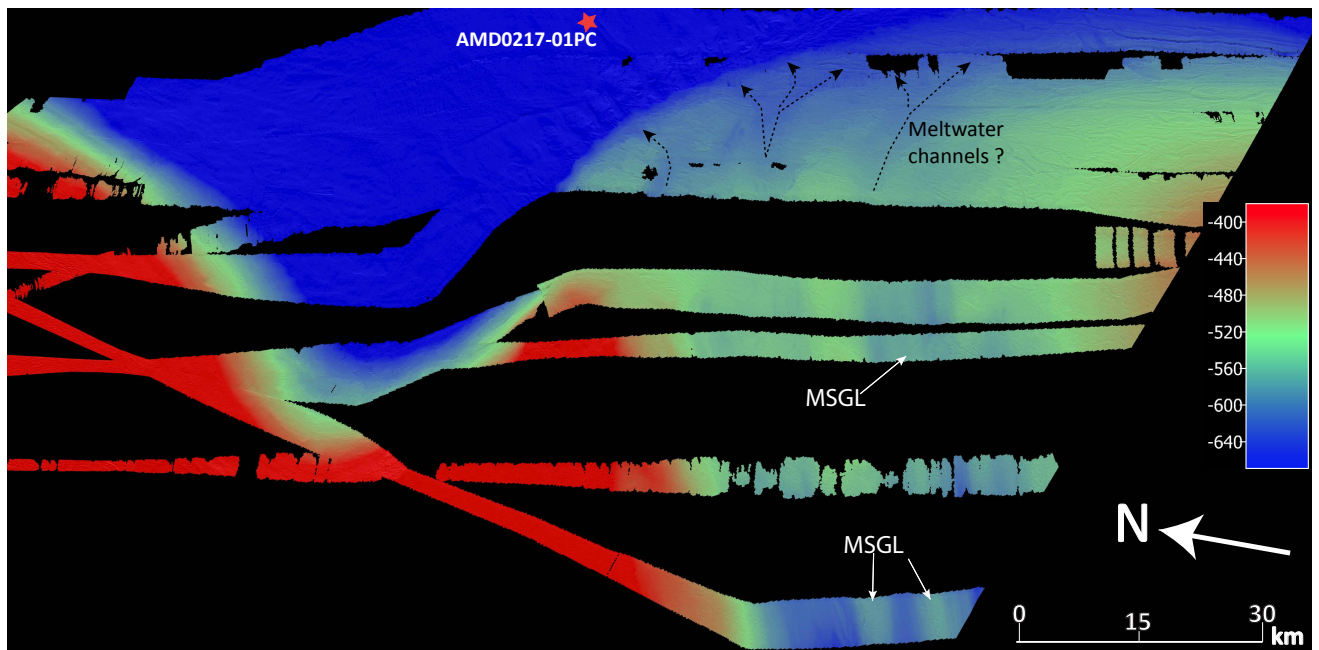




**Figure 9:** Multibeam image of the site of core 1Comp (AMD0217-01) sampled at the edge of a TMF visualized with the QPS Fledermaus software. The white dashed lines represent the delimitation of the TMFs.



**Figure 10:** Multibeam image obtained as part of the ArcticNet program showing mega-scale glacial lineations (MSGs) and iceberg ploughmarks on the shelf. A series of sub-parallel gullies within the slope of Home Bay are also visible and TMFs on the continental rise at the top of the image.



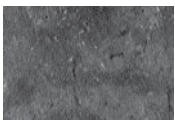

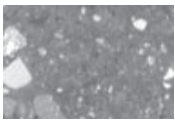

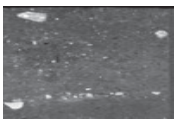

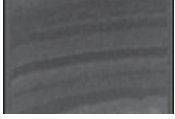

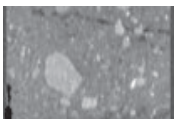

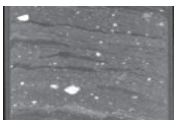



**Figure 11:** Multibeam image software showing MSGLs associated with the activity of the LIS on the shelf during the last glaciation. MSGL are an unequivocal signature of ice stream activity. They are profiled, subparallel and very elongated lineations which are aligned in the direction of the advances and retreat of the LIS. The black dashed lines represent potential meltwater channels.

## 4.2 Lithofacies

Seven lithofacies were identified in the two cores from the TMFs (1Comp and 9CASQ; Figs. 13 and 15). They are described and presented below (see Table 3). The classification of these facies was determined from CAT-scan images, physical and magnetic properties, as well as previous studies from Baffin Bay (e.g. McCann 1988; Tripsanas and Piper 2008; Ó Cofaigh et al. 2013; Simon et al. 2013; Jackson et al. 2017; Jenner et al. 2018).



**Table 3:** Sediment facies characteristics of the cores 1Comp and 9CASQ. From left to right: X-radiographs, high-resolution photography, facies, sedimentary structures and processes with the depositional environment.

X-ray	Image	Facies	Sedimentary	
			Structures	Processes
		Homogeneous mud without IRD (LF7)	Bioturbated grayish to brownish mud without IRD. No apparent structure are observed.	Hemipelagic sedimentation (postglacial)
		Rich carbonate bed with IRD (LF6)	Light olive brown sandy mud and pebbly mud rich in IRD.	Hemipelagic sedimentation with frequent IRD (deglacial/postglacial)
		Homogeneous mud with IRD (LF5)	Dark grayish brown silty mud with IRD. No apparent structures are observable.	
		Laminated mud (LF4)	Dark grayish brown rhythmic succession of mud and silt laminae	Meltwater plume, turbidity current and possible bottom current influence (deglacial)
		Silt and sand turbidite (LF3)	Dense and very dark gray silt and fine sand with clast	Turbidity current (glacial environment)
		Laminated mud rich in IRD (LF2)	Unrhythmic succession of dark gray to dark grayish brown silty laminated mud rich in IRD.	Meltwater plume, ice rafting and turbidity current (glacial environment)
		Complex diamicton (LF1)	Massive, matrix-supported diamict facies. Very dense, black and coarse-grained sediment mixed with a fine-grained matrix.	Glacigenic debris flow (glacial environment)

Photography and CAT-scan reveal a highly variable lithology across the cores (Table 3, Fig. 12). Lithofacies 1 (LF1) is defined as a massive, matrix-supported diamicton facies with very dense, black and coarse-grained sediment mixed with a fine-grained matrix with a sharp upper contact. This facies contain a concentration of granules, pebbles and cobbles which are angular to sub rounded in shape. As previously suggested for similar sediments,

LF1 probably represent GDF triggered near an ice-sheet margin (e.g. King et al. 1998; Ó Cofaigh et al. 2013).

Lithofacies 2 (LF2) is defined as a laminated dark gray to dark grayish brown silty mud rich in IRD with a unrhythmic succession of stratified pebbly mud. The concentrations of pebbles have often deformed the laminae and contacts range from diffuse to sharp (Fig. 12). LF2 facies probably represents sea-ice cover break-ups with renewed warming when iceberg can drift again and the deposition of IRD is re-established (Dowdeswell et al. 2000). LF2 can also be associated with deposition from turbidity currents and turbid meltwater plumes from the ice sheet on the shelf. These layers are often composed of coarse-based laminated mud fining upward (Figs. 13b and 14). Indeed, meltwater may be a major influence on laminated sediment deposition which can be observed in settings relatively proximal to tide-water glaciers reflecting evolution in time in meltwater discharge (Cowan and Powell 1990; Andrews et al. 1991; Dowdeswell and Cromack 1991; Jennings 1993; Dowdeswell et al. 2000; Jenner et al. 2018). This assumption is supported by the fact that during winter or a long phase of climate cooling, ice is covering the entire Baffin Bay which traps icebergs and suppresses their drift offshore. In this case, meltwater discharge will be dominant, when delivery of coarser debris is absent. Cowan et al. (1997) suggested the opposite and proposed punctuated IRD in winter and turbid meltwater deposition dominated by turbidity currents and suspension deposits in summer. One way or the other, deposition of fine-grained laminated glaciomarine sediments are not usually regarded as typical of iceberg-dominated area but sometimes can vary rhythmically with IRD and rapidly deposited layers (Dowdeswell et al. 2000; Domack 1990). Similar layer in core 9CASQ represents a glaciomarine environment. Suspension deposit sedimentation in periods of continuous sea-ice cover has probably generated the mud of this units. The hypothesis of multiyear sea-ice covering the core sites is reinforced by the scarcity of foraminifera, because a continuous sea-ice cover suppresses biological activity (Syvitski 1989; Dowdeswell et al. 2000). Lithofacies 3 (LF3) is defined as dense and very dark gray silt and sand with clast. Facies LF3 are composed of coarse-based laminated mud fining upward. In addition, grain size data highlight the normal grading of this

facies (Fig. 14). The upper contact of this RDL is also visible as shown by the contrast between the finer sediment and the background sediments immediately above (Figs. 13 and 14; e.g. St-Onge et al. 2004; Bourget et al. 2011; Pouderoux et al. 2012). We interpret LF3 has a silty and sandy turbidite. Baffin Island Current (BIC) is particularly strong at 1000-1200 water depth in Baffin Bay Slope (Dunlap and Tang 2006) and that low density muddy turbidity currents can be generated as a result. These proglacial turbidity currents were probably small, dilute and easily dissipated by the BIC. The core 9CASQ, which contain a turbidite deposited in a glacial environment, has been collected at 1220 m below sea level. The strong BIC at this depth might have influence the bottom current deposition and influence the triggering of this type of turbidite (Dunlap and Tang 2006; Roger et al. 2013; Jenner et al. 2018).

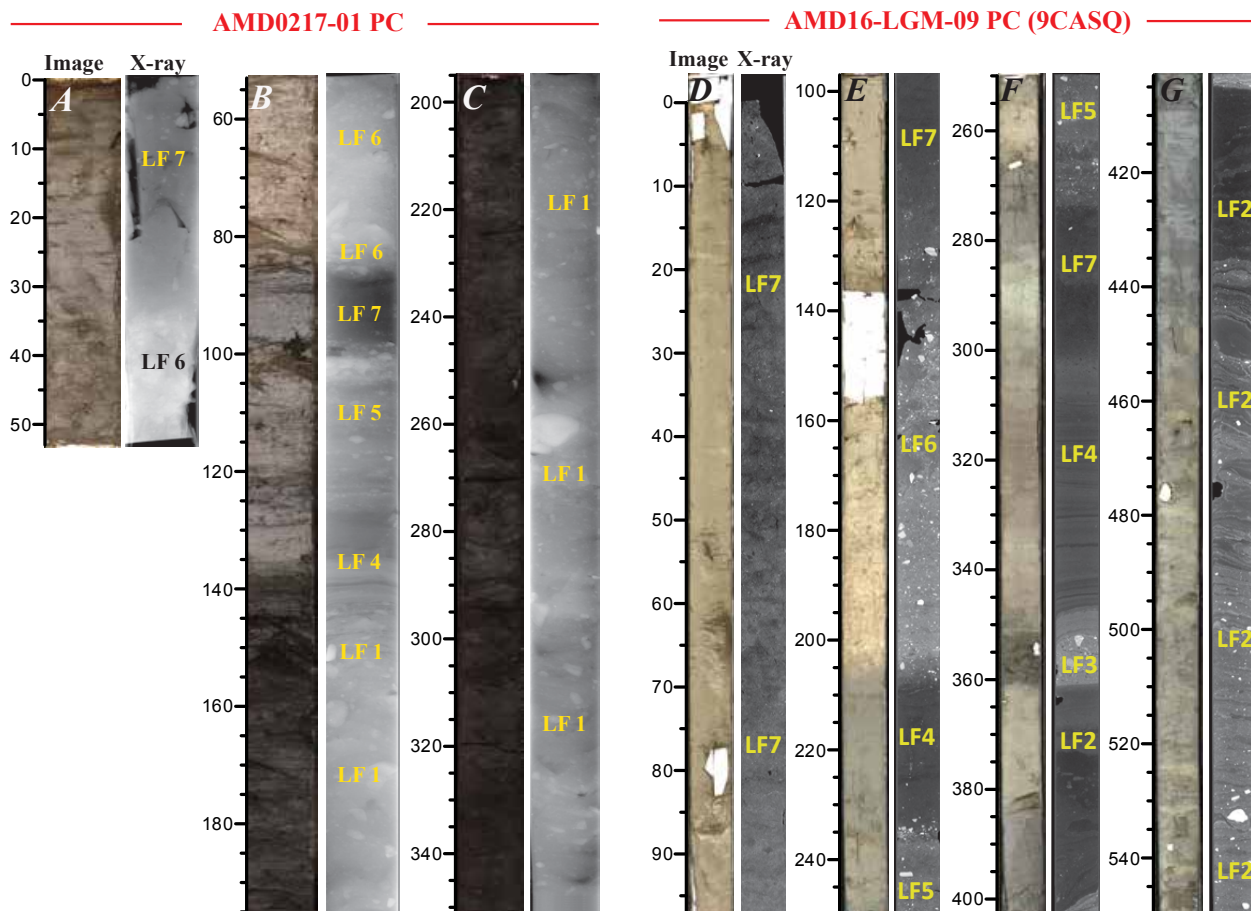
Lithofacies 4 (LF4) is defined as a laminated dark grayish brown rhythmic succession of clay and silt laminae. The laminae and contacts range from diffuse to very sharp and does not contain IRD or bioturbation. As suggested by Jenner et al. (2018), this type of parallel laminations with diffuse contacts can be generated in many ways in northern oceanic environment : by meltwater plumes (Hesse et al. 1997), as mud turbidites seawards of glacial troughs (Roger et al. 2013) and as subglacial outbursts of turbid meltwaters on TMFs (Lucchi et al. 2013). In cores 9CASQ and 1Comp, this facies is mostly overlying a debrite or turbidite and we associate it to muddy density flows and meltwater plumes emanating from glacial discharge during ice retreat.

Lithofacies 5 (LF5) is defined as a massive homogenous dark grayish brown silty mud with the presence of IRD. No apparent structures are observable. The distribution of pebbles within LF5 ranges from dispersed to concentrated and the contacts range from diffuse to gradual. We interpret LF5 as hemipelagic sedimentation with frequent IRDs associated with deglacial/postglacial environment. As IRDs are related to the drifting of icebergs, their presence in cores 1Comp and 9CASQ suggests that a significant portion of Home Bay was ice-free at this time.

Lithofacies 6 (LF6) is defined as a carbonate-rich light olive brown sandy and pebbly

mud with IRD. Previous research has shown that late Quaternary sedimentation seawards of Home Bay is characterized by a proglacial facies containing detrital carbonate that may represent carbonate-rich ice-rafted sediments from northern Baffin Bay icebergs flowing southward with the cold Baffin Island Current and delivering IRDs to the slope between  $\sim 25$  cal ka BP and  $\sim 11$  cal ka BP (Andrews et al. 1998; Andrews et al. 2009; Jackson et al. 2017). Aksu and Piper (1987) suggested that northwestern Baffin Bay, Devon and Ellesmere Islands and northwestern Greenland are the source of the lower Paleozoic limestones and dolomites observed in sediments transported in the form of IRD to southern Baffin Bay (Aksu and Piper 1987).

Finally, lithofacies 7 (LF7) is defined as a massive and homogenous bioturbated grayish to brownish mud without IRD. Apart from traces of bioturbation such as well-defined burrows, no apparent structures are observed (Fig. 12). In contrast with the previous facies rich in ice rafted debris (IRDs), turbidite and debrite, and the presence of this facies in the uppermost part of the core, we associate this facies to hemipelagic sedimentation in a postglacial environment. Similar facies in the uppermost part of cores were also observed along the West Greenland continental margin adjoining Baffin Bay (Dowdeswell et al. 2008; Ó Cofaigh et al. 2013).



**Figure 12:** X-radiographs and high-resolution photography of representative lithofacies from sediment cores of Home Bay TMFs: AMD0217-01 PC and AMD 16-LGM-09CASQ (9CASQ). 1) Massive, matrix-supported diamict facies. Complex diamicton (LF1); 2) Laminated mud rich in IRD (LF2); 3) Silt and sand turbidite (LF3); 4) Laminated mud (LF4); 5) Homogenous mud with IRD (LF5); 6) Carbonate-rich bed with IRD (LF6); 7) Homogenous mud without IRD (LF7). Ticks on the figures represent the depth in cm. See Table 3 for the legend of facies identification and sediment characteristics. N. B. add 30 cm to get the real depths of 1Comp.

### 4.3 Stratigraphy, physical and magnetic properties

#### Core 77PC

Core 77PC is used in this study as a reference core for establishing a reliable chronostratigraphy. Jenner et al. (2018) provided a detailed description of the sedimentary sequence and facies of this core. Overall, this core is composed of laminated and bioturbated mud, wavy silty laminae, detrital carbonate mud and contain no rapidly deposited layers (Jenner et al., 2018). We will now focus on the description of the paleomagnetic results to establish that core 77PC recorded a genuine paleomagnetic signal. Grain size distribution shows relatively fine material with an average of  $\sim 5 \mu\text{m}$  for the entire core (Fig. 15a). Between 161 and 117 cm, a sharp increase of density and MAD values is observed, as well as a decrease in inclination and NRM values. Aside from this interval, the NRM values are relatively constant ( $\sim 0.02 \text{ A/m}$ ), but peaks are seen in the ARM, IRM, and SIRM profiles between 310 and 270 cm, as well as between 470 and 450 cm (Fig. 15a). Nonetheless, MAD values are lower than  $5^\circ$  in the entire core, indicating high quality paleomagnetic data event except for a few intervals. The ChRM has been determined after using a 5 mT demagnetization steps between 10 and 60 mT. The ChRM fluctuates around expected inclination value that was calculated according to the geocentric axial dipole model ( $I_{\text{GAD}}$ ) at the coring site, denoting a well-recorded paleomagnetic signal (Fig. 15a; Stoner and St-Onge, 2007). Downcore MAD values are generally lower than  $2^\circ$ , indicative of very well defined ChRM. The values of the  $\text{MDF}_{\text{NRM}}$  fluctuate between 20 and 40 mT throughout the core with an average of 35 mT. Such an average indicates the presence of low coercivity minerals such as magnetite, except from a few very thin intervals where MDF values close to 50 mT are observed.

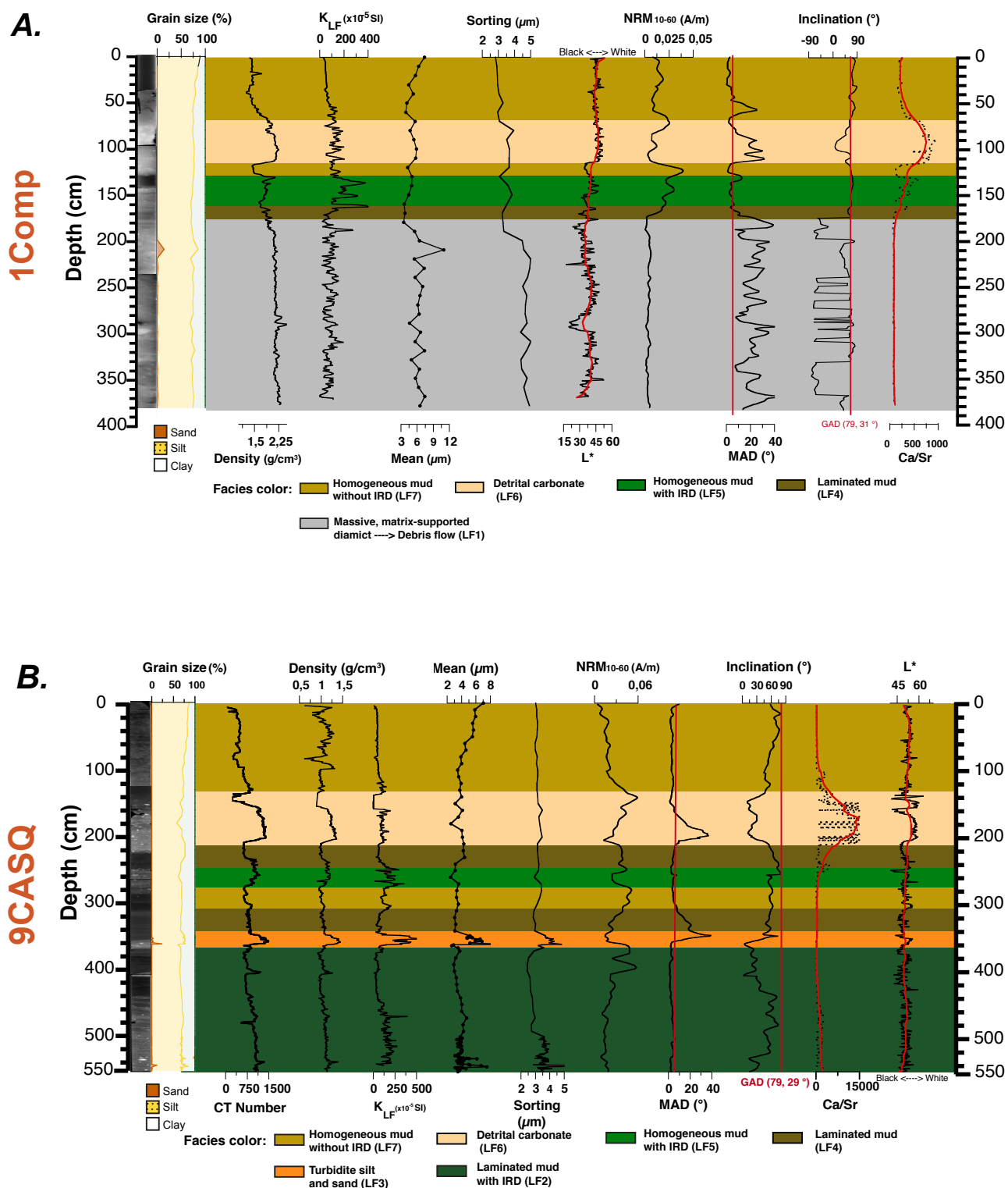
## Core 1Comp

The correlation of density measured on the piston and the trigger weight core 01 suggests that about 30 cm of sediment was lost during piston coring. This missing sediment was taken into account when constructing the composite profile (Fig. S3). The 01 composite sequence is characterized by highly variable lithofacies. The physical and magnetic properties allowed the identification of 5 distinct stratigraphic units (Table. 3 and Fig. 13a). These units represent different sedimentary processes (Fig. 17). The grain size distribution shows relatively constant variations ranging from fine clay to fine sand, except for a peak between 225 and 200 cm which reaches 12  $\mu\text{m}$  and which is consistent with the presence of a debris flow deposit covering the base of the core 1Comp (Fig. 13a). This thick layer (LF1) is less sorted than the overlying sediments. LF1 was observed only in core 1Comp and extends from 381 to 175 cm. The base of this core is firm with high densities ( $\sim 2 \text{ g/cm}^3$ ), black with low  $L^*$  values, matrix-supported with high sorting ( $\sim 5 \mu\text{m}$ ) and mean grain size that vary around 7  $\mu\text{m}$ , predominantly massive diamicton with a sharp upper contact (Table. 3; Figs. 12 and 13a). LF4 extends from 175 to 161 cm, has low magnetic susceptibility, good sorting and mean grain size that varies around 3  $\mu\text{m}$ . The coarse material from LF5 reflects high values of magnetic susceptibility that peaks at about  $400 \times 10^{-5} \text{ SI}$ , which is due to the presence of pebbles containing a high concentration of ferrimagnetic minerals. Unit 5 (LF5) extends from 161 to 129 cm.

The detrital carbonate layers (LF6) from 117 and 65 cm are visible on the CAT-scan images (Fig. 12) and can be identified with other parameters such as  $L^*$ , Ca/Sr ratio, MAD values, inclination and magnetic intensity (Figs. 13a and 15b). The higher  $L^*$  values observed in LF6 most likely reflect a higher carbonate content. This proxy is often used for carbonate content in marine sediment cores (e.g. Balsam et al. 1999; Jackson et al. 2017). The ratio of calcium (Ca) to strontium (Sr) is also frequently used to identify detrital carbonate bed (Hodell et al. 2008; Channell et al. 2012; Winsor et al. 2012). This ratio averages around 100 throughout the core 1Comp, but inside these facies it reaches 750 at 85 cm. In addition,

LF6 between 117 and 65 cm has MAD values reaching  $30^\circ$  at 100 cm, as well as a decrease in inclination and remanence values (NRM, ARM, IRM, SIRM; Fig. 15b). These results attest to the presence of a detrital carbonate layer (Fig. 13a), as well as ice rafting since many clasts are observed in this unit. Similar to 9CASQ, LF7 covers the top of the core between 65 to 0 and from 129 to 117 cm. NRM, ARM, IRM and SIRM values are variable throughout this core with significantly higher values in LF5, suggesting an increase in the ferrimagnetic mineral concentration (Fig. 15b). Inclination values in this unit also fluctuate around the expected values of the GAD with MAD values below  $5^\circ$ , representing high quality paleomagnetic data (Stoner and St-Onge, 2007; Tauxe, 2010). Shallower inclinations and much higher MAD values are observed between 381-175 cm, 161-115 cm and 117-65 cm. These intervals correspond to the bottom debris flow deposit and IRD-rich layers. In the debris flow deposit, the alternance of negative and positive inclination values denotes the presence of clasts (Figs. 13a and 15b). Aside from the debris flow which has low values, the  $\text{MDF}_{\text{NRM}}$  values fluctuate between 30 and 55 mT with an average around 45 mT (Fig. 15b), indicating the presence of low coercivity minerals such as magnetite and a contribution from higher coercivity minerals (Tauxe and Wu 1990; Stoner et al. 2000).





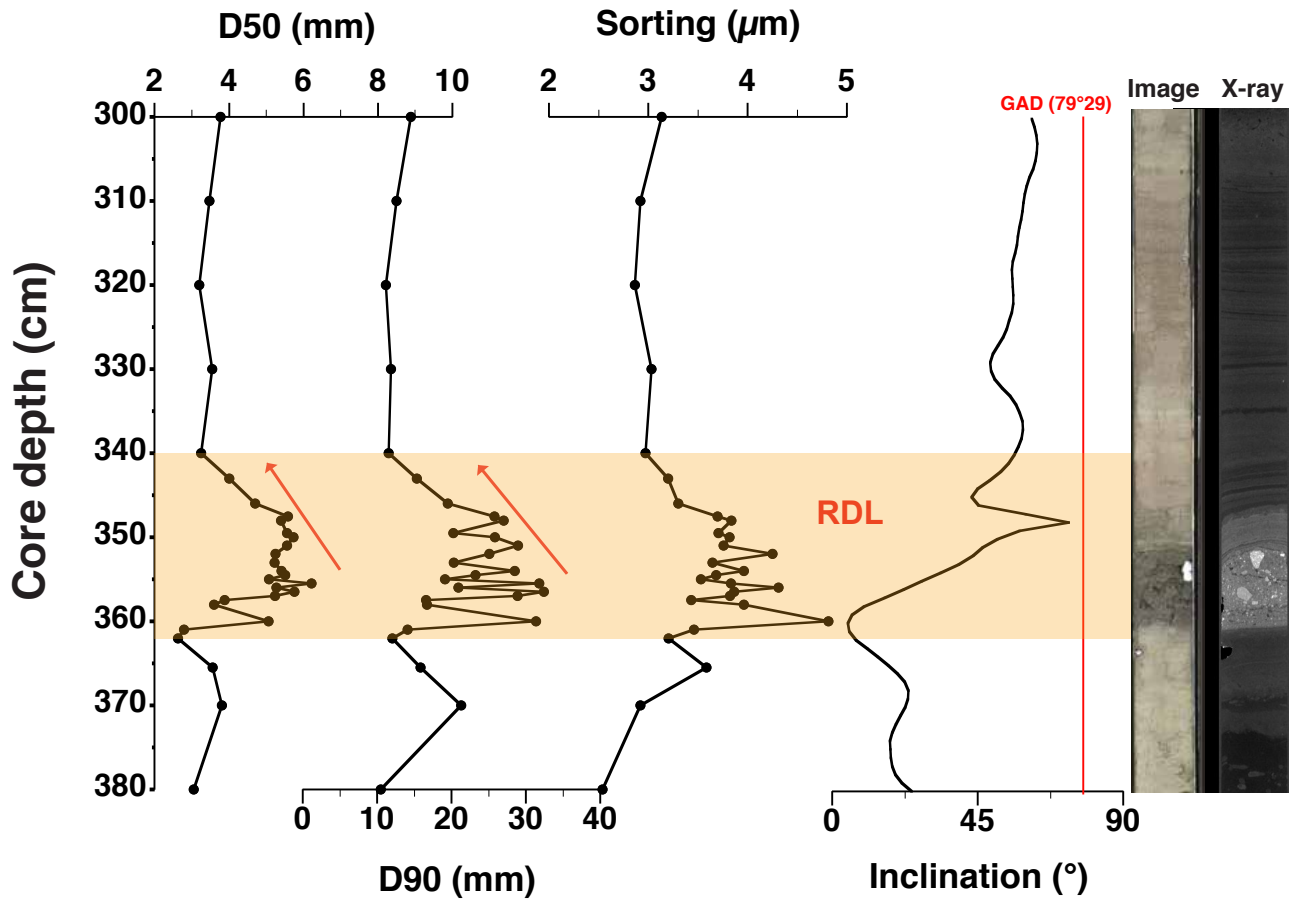
**Figure 13:** High-resolution physical and magnetic properties of cores 1Comp (A) and 9CASQ (B). See text for details. Significant lithological facies are numbered and highlighted with colors (see also Table 3 and Figure 12 for facies description and depositional environment). The vertical red lines delineate respectively the MAD value of 5° and the expected inclination according to geocentric axial dipole ( $I_{GAD}$ ) at the coring site.

## Core 9CASQ

Core 9CASQ is characterized by 6 lithofacies (Table 3, Fig. 13b). The grain size distribution shows relatively constant variations throughout the core ranging from fine clay to coarse silt with an average of 4  $\mu\text{m}$ , except for three distinct layers where the average increases between 544-536 cm, 533-523 cm and 362-340 cm (Figs. 13b and 14), which correspond respectively to LF3 and two thin layers at the base of LF2 which could be turbidites (Table 3, Figs. 13b and 14). These three layers are also less sorted than the rest of the core and they present the normal grading of muddy turbidite (e.g. St-Onge et al. 2004; Bourget et al. 2011; Pouderoux et al. 2012). In addition, for LF3, high-resolution physical and magnetic analyses also revealed the presence of a rapidly deposited layer (RDL) in core 9CASQ and is recognizable by its low basal paleomagnetic inclinations and MAD values (St-Onge et al. 2008; Philippe et al. n.d.). As a whole, LF2 extends between 550-362 cm and is characterized by unrhythmic succession of stratified pebbly mud with often deformed diffuse to sharp parallel laminations, ice rafted debris and probably thin turbidites (Fig. 13b). The coarser base of the turbidite in LF3 are visible on the CAT-scan images (Fig. 12) and are reflected by higher density, CT number and magnetic susceptibility values that can reach  $\sim 400 \times 10^{-5}$  SI (Fig. 13b). LF4 extend over two distinct intervals between 241 to 211 cm and 340 to 305 cm and is laminated with a rhythmic succession of clay and silt laminae.

Lithofacies 5 (LF5) and 6 (LF6) are observed respectively between 275-241 cm and 211 to 125 cm. The coarser material present in these two facies is also visible on the CAT-scan images (Fig. 12). Like core 1Comp, LF6 is characterized by high  $L^*$  values, a sharp increase of the Ca/Sr ratio and lower inclination and MAD values.

LF7 covers the top of the core between 125 and 0 cm, as well as between 305 to 275 cm. LF7 and LF4 reveal little variation in their physical and magnetic properties of the sediments in these facies. Indeed, the density is relatively low, the sorting is good and varies little, whereas the mean grain size is stable and averages 4  $\mu\text{m}$ .



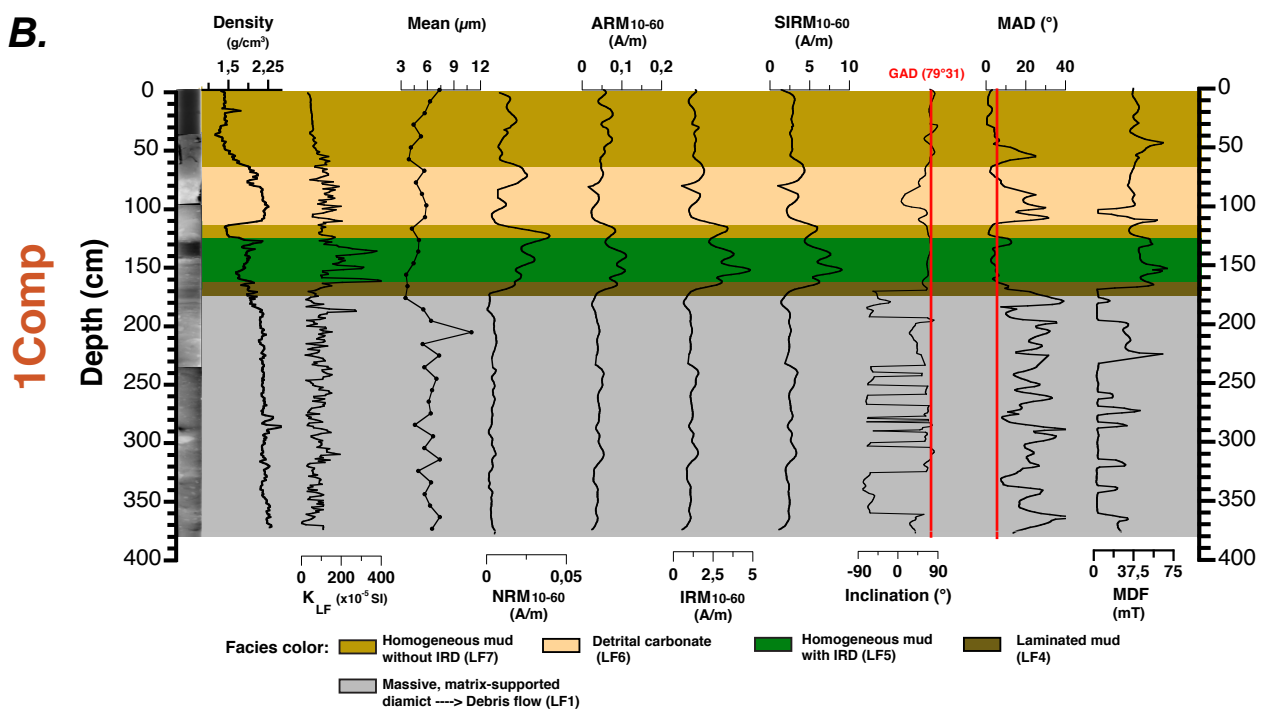
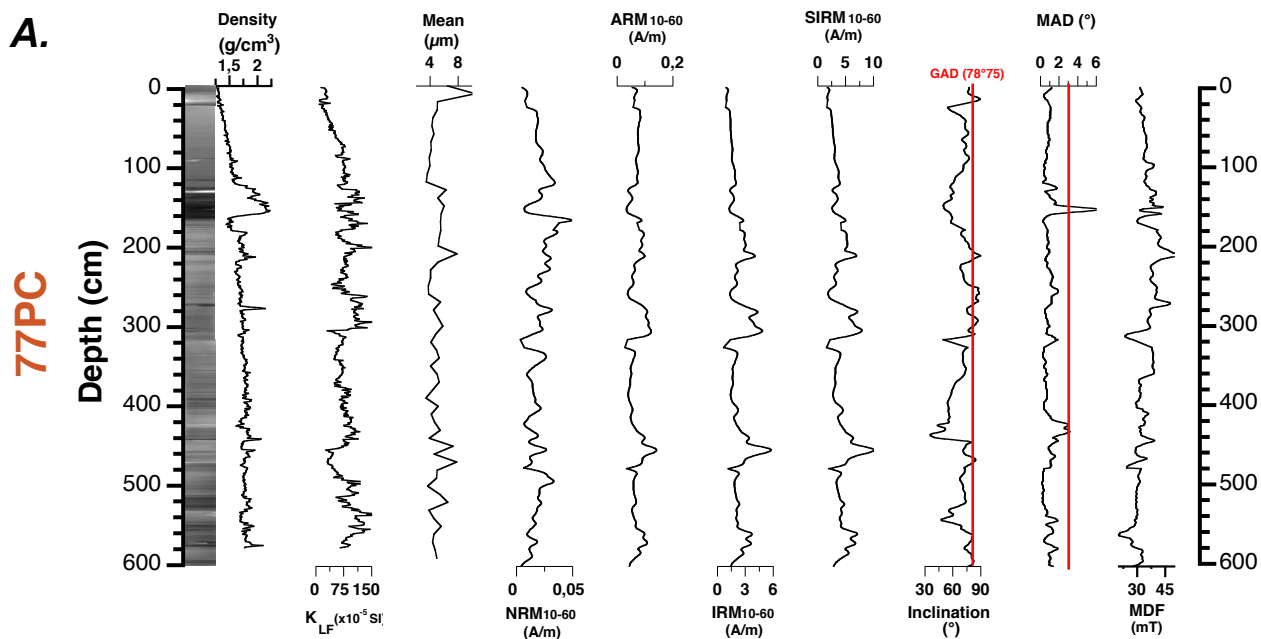
**Figure 14:** Grain size signature (D50, D90, sorting) and inclinations of LF3 in core 9CASQ sampled in the lower continental slope of Home Bay. These trends illustrated the normal grading of a turbidite. The orange layer represent the RDL facies.

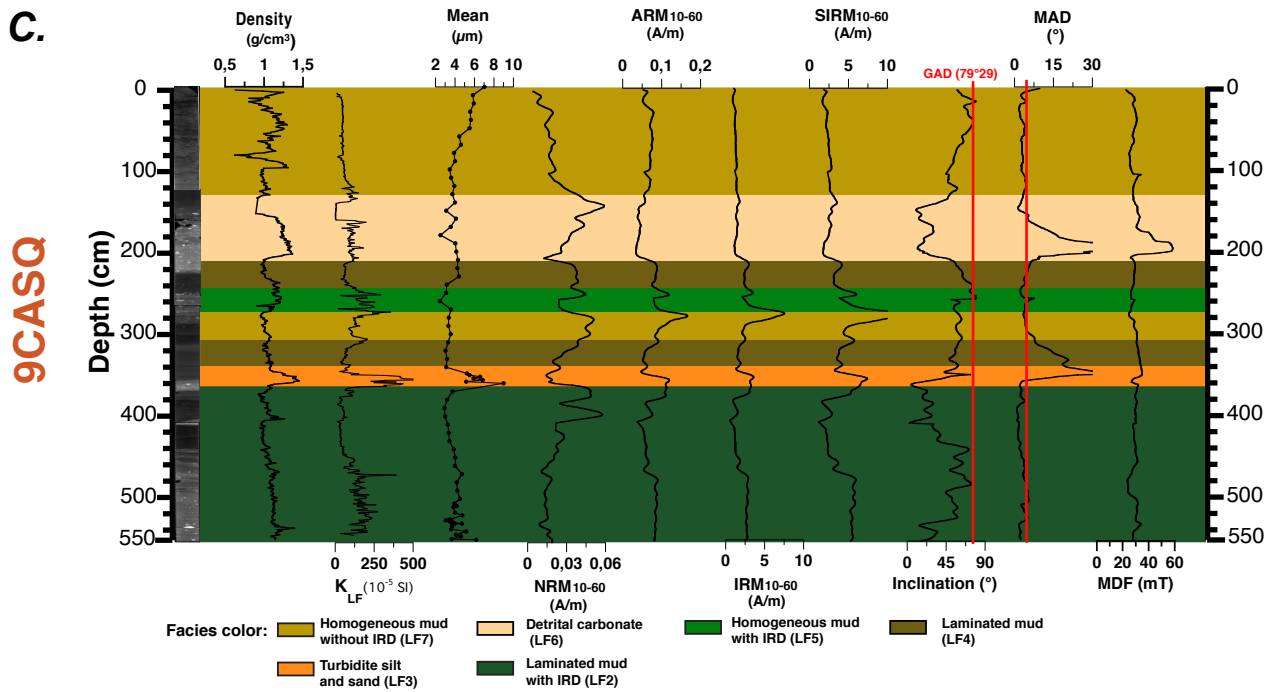
The ChRM inclination along the core generally fluctuates around the expected inclination values ( $I_{GAD}$ ) and MAD values are lower than  $2^\circ$ , indicative of very well-defined paleomagnetic data, except for the detrital carbonate and turbidites layers (LF6 and LF3), which have low inclination and high MAD values. Aside of the LF6 layer,  $MDF_{NRM}$  values range between 20 and 40 mT with an average of 30 mT, which is indicative of the presence of low coercivity minerals such as magnetite throughout the core (Fig. 15c). The sharp increase in MDF values in the detrital carbonate layer indicates a lower concentration of magnetite and the presence of higher coercivity minerals in this layer (Simon et al. 2012).

#### 4.4 Magnetic properties

Day plots indicate that most of the sediments of the three cores are composed of magnetic grains in the pseudo single domain (PSD) range although some samples of cores 1Comp and 9CASQ fall in the multi domain range (MD). The samples in the MD range reflect the coarser grains observed in the rapidly deposited layers (e.g. turbidite and debrite). For the three cores, the magnetic  $k_{\text{ARM}}/k$  diagram (King et al., 1983) indicate that the magnetic grain size is relatively fine and under  $5 \mu\text{m}$ . Even though, the absolute magnetic grain size values are to be taken with caution as these empirical relationships were carried out for synthetic magnetic grains, taken together with the results from the Day plot, they suggest an optimal PSD range for paleomagnetic reconstructions (e.g. Tauxe, 1993).

The shape of hysteresis curves of the discrete samples from the three cores are typical of low coercivity ferrimagnetic minerals such as magnetite (Fig. 16a; Tauxe et al. 1996; Dunlop and Özdemir, 1997). In addition, the magnetic mineralogy-dependent ratio  $\text{IRM}/\text{SIRM}$  (Pseudo S-ratio) is useful to estimate changes in magnetic mineralogy, with values close to 1 indicating a low-coercivity ferrimagnetic mineralogy (e.g. magnetite; St-Onge et al., 2003). The S-ratio in cores 77PC, 1Comp and 9CASQ, with mean values of 0.992, 0.988 and 0.987 respectively, suggesting that low coercivity minerals such as magnetite is the dominant magnetic carrier. Moreover,  $\text{MDF}_{\text{NRM}}$  values ranging from 25–40 mT also suggest the presence of magnetite and/or titanomagnetite in most of the 3 cores (Fig. 15). On the other hand, sediments of LF1 and LF6 in core 1Comp are characterized by lower MDF values that indicate the occurrence of coarser magnetic grains as seen in the Day plot (Fig. 16b) and physical grain size data (Fig. 16c). Finally, changes in NRM, ARM, IRM and SIRM vary by less than an order of magnitude.

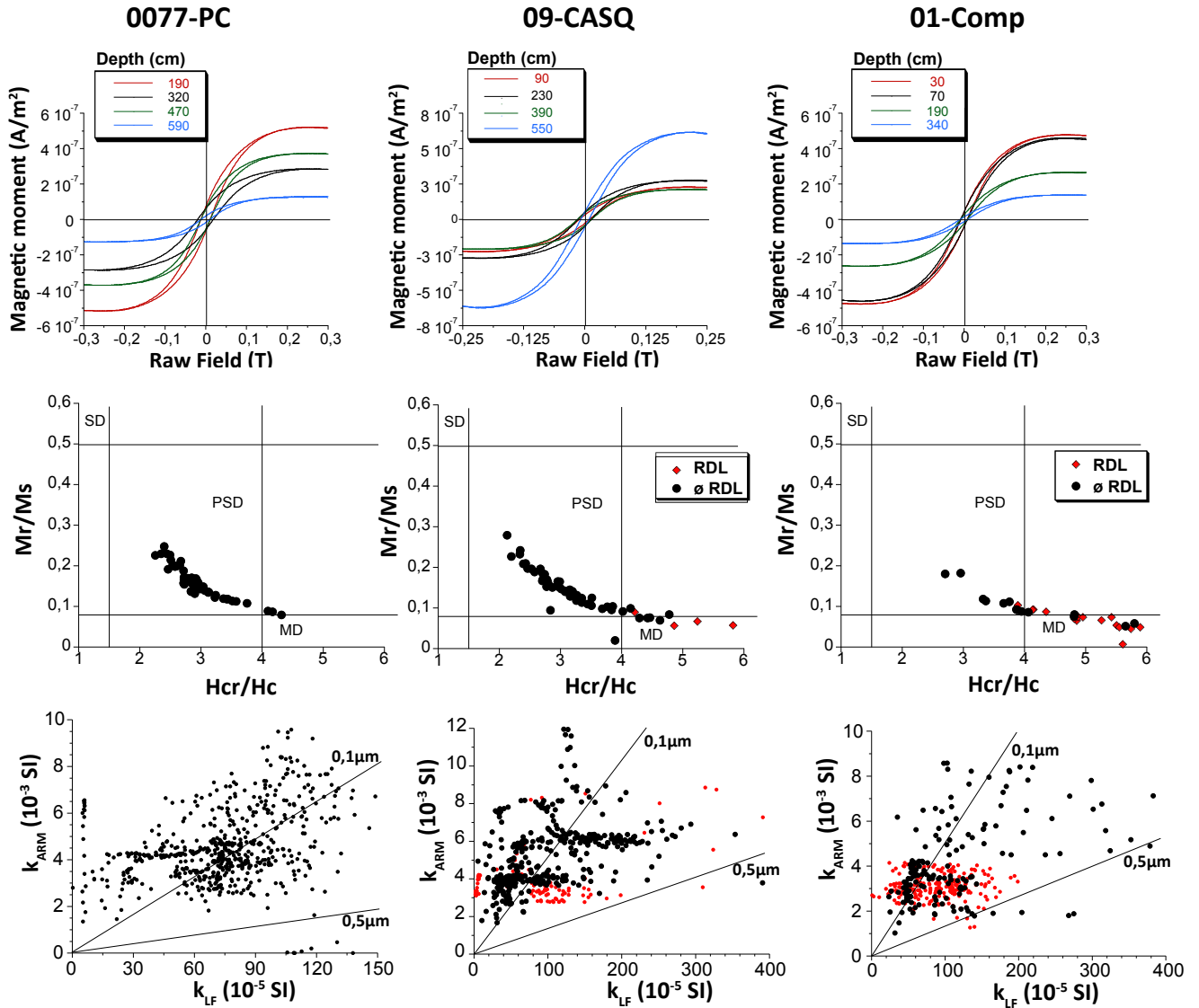




**Figure 15:** . High-resolution physical, geochemical and magnetic properties of cores 77PC (A), 1Comp (B) and 9CASQ (C). See the text for details. Distinct lithological facies are numbered and highlighted with colors. Gray: massive, matrix-supported diamicton facies => Debris flow (LF1); Dark green: Laminated mud rich in IRD (LF2); Orange: silty and sandy turbidites (LF3); Dark brown: Laminated mud (LF4); Pale green: Homogenous mud with IRD (LF5); Beige: detrital carbonate rich in IRD (LF6); Yellow brownish: homogeneous mud without IRD (LF7). See Table 3 for more details on facies identification.

#### 4.5 Relative Paleointensity (RPI) Determination and Chronostratigraphy

To derive a RPI proxy, some criteria must be satisfied : the NRM must be characterized by a strong, stable, single component magnetization with MAD values < 5°, carried by low coercivity ferrimagnetic grains (e.g. magnetite) in the SD/PSD domain (e.g. Levi and Banerjee 1976; Tauxe 1993; Stoner and St-Onge 2007; Yamazaki et al. 2013). Moreover, magnetite concentration variations should not vary by more than a factor of 10 (Tauxe, 1993). The NRM should also be normalized by an appropriate magnetic parameter (normally ARM or IRM) that activates the same grains that carried the NRM (Levi and Banerjee, 1976). The relative



**Figure 16:** A. Typical hysteresis curves and derived parameters of cores 77PC, 9CASQ and 1Comp; B: Day plot (Day et al. 1977): RDL= Rapidly deposited layers (turbidite and debrite); C:  $k_{ARM}$  vs.  $k_{LF}$  plot representing estimated magnetic grain size for magnetite (King et al. 1983): Red circle represent RDL and black circles the remaining sediments.

paleointensity proxy cannot be correlated with its normalizer or with any lithological proxy (Tauxe and Wu, 1990). For cores 77PC, 1Comp and 9CASQ, the comparison between ARM and IRM as normalizers seem to activate the same magnetic assemblages and the difference between ARM and IRM as normalizers also suggest that ARM have a slightly better  $R^2$  then

IRM (Figs. S1 and S2). For the 3 cores, the comparison of the normalized remanence with its normalizer indicates that NRM/ARM is not correlated with the ARM when RDL are excluded (Fig. S1). Conversely, the same comparison indicates a correlation for RDL (e.g. debrite and turbidite; LF1 and LF3) and detrital carbonates (DC) layers (LF6) with  $R^2$  of respectively 0.37 and 0.40 (Fig. S1). Based on these results, ARM has been selected as the best normalizer. Detrital carbonate layers were then excluded for paleomagnetic reconstructions, but RDL, even if they do not yield appropriate results, have been kept in the figures in order to give the reader a glimpse of their age-depth relationship.

## 5 Discussion

### 5.1 RDL layers: Glaciogenic debris flows (GDFs) and turbidites

Glaciogenic debris flows are major components of TMFs (e.g. Laberg and Vorren 1995; King et al. 1998; Vorren et al. 1998; Nygard et al. 2002). In Home Bay, LFI is characterized by a massive, matrix-supported diamicton facies with clasts, the highest MAD values and low values of paleomagnetic inclinations (Fig. 15b). This combination of parameters clearly indicate that glaciogenic debris flows were recorded. Magnetic properties of sediments can be a source of significant information for the interpretation of sedimentary products. In fact, turbidites, debrites and detrital carbonate layers generate higher MAD values ( $> 5^\circ$ ) and highly variable inclinations which move away from the expected values. If the inclination is highly variable very shallow such as in the debrite (LF1) of core 1Comp and in the turbidite (LF3) in core 9CASQ, it has no geomagnetic meaning, but clearly indicates the presence of a rapidly deposited layer (RDL).

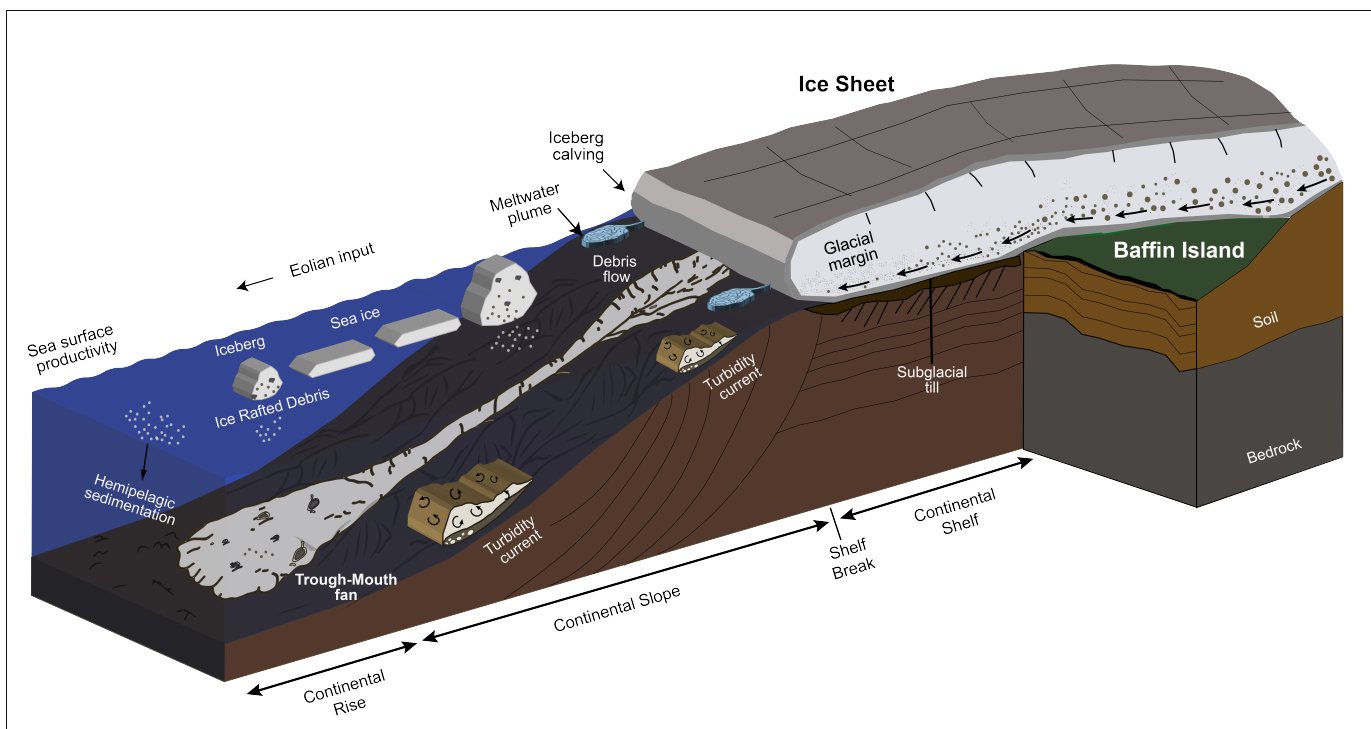
A series of stacked debrites encompasses a wide range of scale, geometry, structure, lithology and process. They have specific shape and geometry and they usually accumulate in the form of continuous and elongated lenses inside a TMF (Nygard et al. 2002). The



final depositional area are often observed at great distances from the origin (De Blasio et al. 2006) and have volumetric importance and ubiquitous distribution in high latitudes that reflect past glacial environment (King et al. 1998; Nygard et al. 2002; Ó Cofaigh et al. 2013). Turbidity currents are also gravity-driven density currents and occur on continental slopes as well as adjacent parts of ocean basins. They are considered, along with debris flows, to be one of the main processes of sediment transfer in deep oceans (Piper and Normark 2009). They are generally triggered when an event occurs such as a seismic event, landslide, high sedimentation rates or ice sheet movements near the shelf edge (Li et al. 2012; Talling et al. 2013; Talling 2014). Moreover, according to past studies, debris flows sometimes evolve distally into turbidity currents (Nemec 1990; De Blasio et al. 2006; Talling et al. 2007).

Both physical and magnetic profiles of the core 9CASQ highlight the presence of a turbidite along the slopes of Home Bay in the most distal part of a small TMF. This core, recovered in a distal area of a TMF (Fig. 8) about 100 km away from the coast, contains a turbidite between 362 and 340 cm. This turbidite contrast sharply with the dark grayish brown silty mud of hemipelagic sedimentation and IRD layers associated to the continuous "background" sedimentation (Figs. 13b and 14). The presence of debrites and turbidites attests to the sensitivity of Home Bay to capture mass wasting events that can be associated with advances of the LIS on the shelf edge (Fig. 17). This type of sediment therefore represents a glacial environment, while IRD deposits are more associated with periods of warming and melting ice during ice sheet retreat. Laberg et al. (1995) have reported the same association of sedimentary processes during the LGM where large debris flows have been generated and accumulated down the slope on the Bear Island trough-mouth fans when the Barents Sea Ice Sheet reached the shelf break (Laberg and Vorren 1995). They identified a chronological sequence of debrites which have accumulated inside a North Sea Fan. This sequence corresponds to the advances and retreats of the southern Fenoscandian Ice Sheets from 18 to 15 ka BP and GDFs are directly associated with the presence of the inlandsis at the shelf break (Fig. 17; King et al. 1998). Subbottom profiles from the sampling location of core 1Comp (Figs. 2 and 9) reveal that the acoustic facies associated with the debris flow extends laterally

to a series of stacked debris flow deposits which accumulated inside this TMF (Fig. 5). In addition, subglacial landforms like MSGL and iceberg ploughmarks reveal a complex and dynamic layer of ice and subglacial ice stream that suggests a glacial calving margin on the shelf during the Last glacial episode. On the other side, the available data do not confirm the presence of GZW in the sector of Home Bay trough (Fig. S4) that could testify the presence of an ice sheet on the continental shelf (Batchelor and Dowdeswell 2015). Most of the iceberg ploughmark scars are likely caused by icebergs coming from Greenland, but they might also suggest the presence of a glacial calving margin at the shelf during the LGM (Dowdeswell et al. 1993; Dowdeswell and Ottesen 2013). These features are found at a depth of about 650 m and are frequently oriented in a north-south direction, like the BIC (Fig. 10). This orientation along the BIC suggests that these iceberg ploughmarks could also have come from northern Baffin Bay and would have drifted south along the coast of Baffin Island to run aground on the continental shelf of the sector. MSGLs landforms are signature of ice stream activity and several meltwater channels have probably been used as feeder corridors for TMFs systems (Fig. 11; Ottesen et al. 2005; Montelli et al. 2017). Furthermore, these meltwater channels can be used to determine the direction of past ice-flow to the shelf break during glaciation. Sediments are transported by this ice stream and can also travel downslope as a series of debris flows (e.g. Laberg and Vorren 1995; Lasabuda et al. 2018) and turbidity currents. Several small canyons and gullies will eventually serve as the main transport routes for remobilizing sediments from the upper slope towards their accumulation site in the basin (e.g. Lasabuda et al. 2018) as TMFs (Figs. 8 and 9). These multiple erosional surfaces (scars) suggest glacial processes have eroded and molded the shelf during the Quaternary. There is no evidence these structures were generated during the Last glacial episode (or even during the LGM), but this strong glacial erosion not covered by thick layers of sediments on the continental shelf, as well as the morphology of the seabed and the stratigraphy of a glaciogenic debrite and turbidite dated from the last glaciation ( $\sim 15$  and  $20$  cal ka BP; Fig. 18), suggest the LIS margin extended to the shelf edge during the LGM. These results, paired with the dating of a glaciogenic debrite and turbidite, demonstrate the activity of glacial processes near the shelf



**Figure 17:** Schematic model for the main glaciogenic sedimentary processes inside a trough-mouth fan (TMF).

edge.

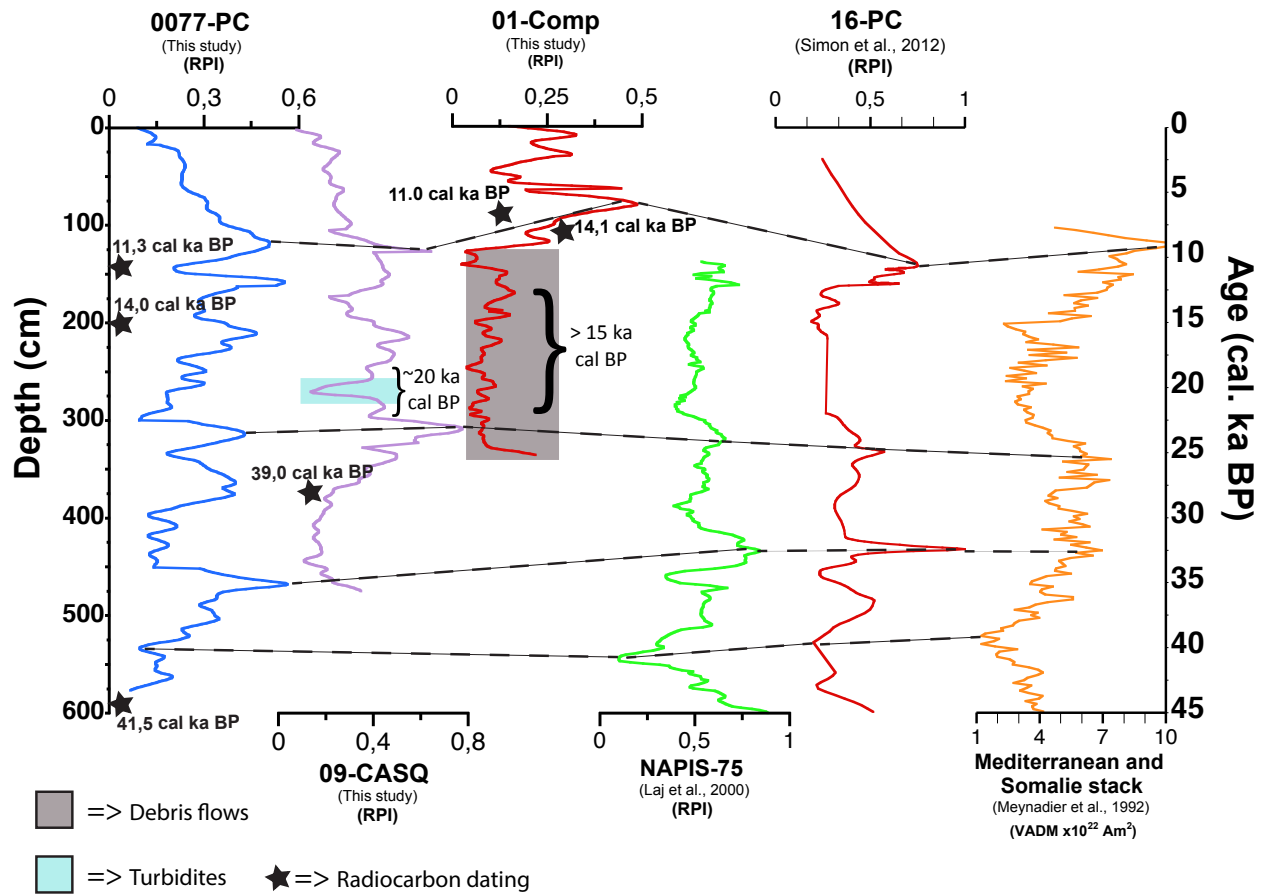
## 5.2 Late Pleistocene Baffin Bay chronostratigraphy

In order to date these debrite and turbidite and to establish an original age-depth relationship for these cores in Home Bay, a combination of radiocarbon ages along with paleomagnetic tie points were used to determine the chronology of these cores. These 3 cores show similar directional and relative paleointensity (RPI) features that can be correlated on a regional scale and with other Northern Hemisphere paleomagnetic secular variation (PSV) records at the millennial scale since the last 45 ka (Fig. 18).

Figure 18 shows the comparison of RPI profiles from 0 to 580 cm in core 77PC, 0 to 475 cm in core 9CASQ, and from 0 to 337 cm in core 1Comp along with 3 previously published

RPI records from the Northern Hemisphere: North Atlantic stack (NAPIS-75; Kissel et al. 2000; Laj et al. 2000), Baffin Bay (Core 16PC, Simon et al. 2012) as well as Mediterranean and Somali Stack (Meynadier et al. 1992). This comparison supports the geomagnetic origin of the signal in the 0–45 ka interval for cores 77PC, 9CASQ and 1Comp, as well as to support the available radiocarbon ages.

According to this comparison and the dating model, we suggest that the debrite observed in core 1Comp were triggered before 15 cal ka BP, while the turbidite (LF3) of core 9CASQ were deposited around 20 cal ka BP. Furthermore, subbottom profiles (3.5 kHz) from the coring site of core 1Comp illustrates that the core was collected on the side edge of a debris flow channel (Figs. 5 and 9) in a much thinner section ( $\sim 4$  m depth) than the center of this channel which is more than 10 m deep (Fig. 5) and probably dating back, at its deepest, to more than 15 cal ka BP. The chronostratigraphy thus suggests that debrite and turbidite observed within cores 1Comp and 9CASQ are glaciogenic origin. Without disqualifying the possibility of an earthquake in the Baffin Bay area at this time, the turbidite found in core 9CASQ were dated from the Last glacial episode ( $\sim 20$  ka BP) and are more likely to have been triggered by the presence of the LIS margin on the continental shelf. Previous work has shown that large volumes of turbidites along ice margins are essentially related to subglacial outbursts and can be used as a proxy to determine a glaciomarine source (Dowdeswell et al. 1998; Hesse et al. 1999; Toucanne et al. 2012). There is still no general agreement on which sedimentary structures can be used to distinguish fine-grained turbidites from contourites (Rebesco et al. 2014) and it has been a controversial issue in sedimentology since the 1970's (Hollister 1967; Piper 1972; Hollister and Heezen 1972). Some authors have already considered that fine turbiditic deposits like LF3 in core 9CASQ can be differentiated from contourite based on certain characteristics: the absence of widespread burrowing, bioturbation, a lack of a vertical sequence of structures (Lovell and Stow 1981; Stow and Piper 1984) and traction sedimentary structures (Carter et al. 1996; Wynn and Stow 2002; Shanmugam 2006). These criteria are considered to be viable diagnostic for differentiated fine turbidites from contourites. Furthermore, the combination of the data (timing, mega-scale glacial lineations,



**Figure 18:** RPI correlation. Relative paleointensity inter-comparison for the last 45000 cal BP between cores 77PC (this study), 9CASQ (this study), 1Comp (this study) and RPI reference curves from North Atlantic stack (NAPIS-75; Kissel et al. 2000; Laj et al. 2000), Baffin Bay (Core 16PC; Simon et al. 2012) as well as Mediterranean and Somali Stack (Meynadier et al. 1992). Correlative paleointensity features are indicated with dashed black line. RDLs (e.g. debrite and turbidite) are delimited by the grey and blue square. Radiocarbon ages from core HU2013-029-0077 have been taken from (Jenner et al. 2018).

TMFs, sedimentology and low inclinations) presented in this paper clearly demonstrate that the graded sediments in LF3 is a glaciogenic turbidite. The very low inclinations at the base of this turbidite is a very strong argument and was previously seen in several records (Fig. 9; e.g. St-Onge et al. 2004; Tanty et al. 2016). Furthermore, the seismic profiles in the area do not present the acoustic attributes of contourites.

### **5.3 New delimitation of the maximum extension of the LIS in Home Bay during the Last glacial episode**

In order to generate GDFs and turbidity currents that have accumulated in the Home Bay TMF at the bottom of the continental slope of Baffin Island, the ice sheet had to advance to the shelf edge during the Last glacial episode. The morphology of the bedforms observed within the area of the Home Bay based on swath bathymetry imagery supports this hypothesis by showing the cross-shelf trough were glacially eroded and contain ice sheet and iceberg scours. Some area also contains MSGs extending to the shelf break, which are indicators of fast ice-flow and are a common signature of ice stream activity (Figs. 10 and 11; Stokes and Clark 2002; Clark et al. 2003; Brouard and Lajeunesse 2017). Their well-preserved morphology and the thin cover of postglacial sediments suggest that they are related to the Last glacial episode. According to some authors, the maximum extension of the LIS in the Home Bay area probably lasted up to 13 - 12 cal ka BP (Dyke et al. 2002; Margold et al. 2015).

These ice-contact landforms, the glaciogenic debrite and turbidite mapped on the Home Bay continental rise and shelf allows us to propose a new delimitation of the maximum extension of the LIS margin in central-western Baffin Bay during the Last glacial episode (Fig. 2), more precisely at the time corresponding to the initiation of the debris flow deposit and the turbidite, which are respectively, according to the age model, during the LGM.

## **6 Conclusions**

The new geomorphological, stratigraphic and sediment core data coupled with the dating of a glaciogenic debrite and turbidite accumulated in trough-mouth fans during the Last glacial episode allow the reconstruction of the activity of the LIS margin in Home Bay trough and trough-mouth fans.

In this paper, three key results allow us to suggest that an ice margin has extended near the shelf edge of Home Bay during the Last glacial episode:

1) 7 facies in three sedimentary cores can be genetically related to different depositional environments associated to the last glaciation and deglaciation. These facies reflect four major depositional environments: A) rapidly deposited layers such as a debrite and turbidite generated in a glacial environment; B) meltwater plumes, turbidity currents and possible bottom current influence generated in a glacial and deglacial environment; C) Ice Rafted Debris (IRD) deposited during the last deglaciation and during postglacial times; D) postglacial hemipelagic sedimentation.

2) The established chronostratigraphy indicate that the debrite and turbidite recorded at the base of cores 1Comp and 9CASQ were probably transported along the slope during the Last glacial episode. They represent a prograding depositional system which eventually accumulated at the bottom of the continental slope as TMFs due to the accumulation of large volumes of glacial sediments. TMFs are considered as evidence of the presence of the LIS margin on the shelf edge.

3) High-resolution multibeam bathymetry allowed the identification of shapes and structures related to ice stream activity near the shelf edge. These subglacial landforms, such as mega-scale glacial lineations, along with the dated debrite and turbidite suggest that these glacial processes have eroded and molded the shelf during the Last glacial episode, allowing us to propose a new delimitation of the maximum extent of the LIS in the Home Bay sector.

Finally, new sediment cores should also be collected from the TMFs adjacent to cores 9CASQ and 1Comp in order to identify and date more turbidites and debrites. Similarly, a new seismic and multibeam survey further upstream in the Home Bay area could also help to accurately delineate the MSGs left by the passage of the LIS in this region. Finally, this paper illustrates the usefulness of combining paleomagnetic measurements with radiocarbon dating to establish a reliable chronostratigraphy in an environment where calcium carbonate

dissolution challenges the use of foraminifera for dating.

**Index of abbreviations-** TMF: trough-mouth fan; GDF: glaciogenic debris flows; LIS: Laurentide Ice Sheet; IIS: Innuitian Ice Sheet; GIS: Greenland Ice Sheet; LGM: Last Glacial Maximum; BIC: Baffin Island Current; 9CASQ: AMD16-LGM-09; 1Comp: AMD0217-01PC and AMD0217-01BC; 77PC: HU2013-029-0077; LF1 to LF7: Lithofacies 1 to 7; RDL: rapidly deposited layer; BBDC: Baffin Bay detrital carbonates; GZW: grounding-zone wedge; MSGL: mega-scale glacial lineation; MSCL: Multi Sensor Core Logger; XRF: X-ray fluorescence. Paleomagnetic parameters: kLF: magnetic susceptibility; NRM: natural remanent magnetization; ARM: anhysteretic remanent magnetization; IRM: isothermal remanent magnetization; SIRM: saturation isothermal magnetization; ChRM: characteristic remanent magnetization; MAD: maximum angular deviation; MDF: median destructive field; IGAD: axial dipole model; PSD: pseudo single domain; SD: single domain; PSV: paleomagnetic secular variation; RPI: relative paleointensity; Ms: saturation magnetization; Hc: coercive force; Mrs: saturation remanence; Hcr: coercivity of remanence; AMS: accelerator mass spectrometry; AGM: alternating gradient force magnetometer; AF: alternating field; DC: direct current



**Acknowledgements-** We thank Calvin Campbell from the Geological Survey of Canada for access to core 77PC and its radiocarbon ages. We also sincerely thank the captains, officers, crew and scientists on board of CCGS Amundsen for the recovery of the cores used in this study. We also thank Quentin Beauvais (ISMER) and Marie-Pier St-Onge (ISMER) for their technical support and advice in the laboratory, and to Jean-Carlos Montero-Serrano (ISMER) for his help collecting some of the studied cores. Thank is also due to Etienne Brouard for fruitful discussions. This research was funded by ArcticNet Network of Centres of Excellence of Canada and by the Natural Sciences and Engineering Research Council of Canada (NSERC) through Discovery grants to G. St-Onge and P. Lajeunesse. Finally, we are thankful to Calvin Campbell, Amando Lasabuda and Kimberley Jenner for providing constructive reviews.



## CONCLUSION GÉNÉRALE

Ce projet de maîtrise a permis de définir une nouvelle extension maximale de l’Inlandis laurentidien (IL) dans la région de Home Bay grâce à la morphologie des fonds sous-marins et aux turbidites et coulées de débris accumulées dans les éventails glaciogéniques (EGs) au cours de la dernière glaciation.

Huit lithofaciès représentatifs d’un système EGs ont été identifiés dans les carottes de Home Bay sur la base des différentes propriétés des sédiments et des images CT-scan. Ces lithofaciès sont d’un grand intérêt pour mieux comprendre les séquences sédimentaires et les processus liés à la dynamique de la dernière glaciation et déglaciation. Les lithofaciès à la base des séquences sédimentaires des carottes sont principalement constitués : 1- Un faciès massif qui contient une matrice de boue sableuse riche en diamictons qui provient des coulées de débris glaciogéniques déclenchées dans un environnement glaciaire ; 2- Un faciès de boue laminée et/ou massive à base grossière et qui s’amincit progressivement vers le sommet de la séquence. Ce faciès reflète des turbidites déposées dans un environnement glaciaire.

Les trois autres faciès sus-jacents sont constitués de boue bioturbée (sédimentation hémipélagique) contenant occasionnellement des cailloux, une boue laminée parsemée de cailloux (sédimentation hémipélagique avec des débris délestés par les icebergs (IRD) et une boue laminée (sédimentation hémipélagique sans débris délestés par les icebergs (IRD) qui représentent respectivement des environnements de déglaciation et postglaciaires. Ces faciès sédimentaires sont également visibles sur les profils sismiques (3,5 kHz) et sont caractérisés par des unités acoustiques stratifiées représentant une alternance de boue et de coulées de débris/turbidites surmontées par une unité acoustique transparente représentant des boues postglaciaires.

Les résultats paléomagnétiques obtenus sur des u-channels ainsi que les données d’hystérésis des carottes HU2013-029-077 (77PC), AMD16-LGM-09 (9CASQ) et

AMD0217-01 (1Comp) révèlent que les sédiments de Home Bay sont des enregistrements paléomagnétiques de haute qualité dont l'aimantation est portée par des minéraux de faible coercivité comme la magnétite de type pseudo-single domain (PSD). La magnétostratigraphie et les datations radiocarbone sur les carottes des EGs de Home Bay indiquent que les coulées de débris glaciogéniques et les turbidites remontent à plus de 15 cal ka BP, et donc, du dernier épisode glaciaire. En effet, selon Dyke et al., (2002) et Margold et al., (2015), l'extension maximale de l'Inlandsis laurentidien dans la région de Home Bay aurait probablement duré jusqu'à 13 000 - 12 000 BP.

Ces résultats indiquent qu'une série de coulées de débris et de turbidites ont été générées durant la dernière glaciation, suggérant que la marge glaciaire de l'IL a atteint la limite du plateau, tandis que la sédimentation postglaciaire a conduit au dépôt principalement de boues hémipélagiques bioturbées et/ou caillouteuses et laminées.

De plus, de multiples surfaces d'érosion (cicatrices) démontrent l'activité des processus glaciaires antérieurs sur le plateau continental et la présence de linéation glaciaires à grande échelle (MSGL) qui s'étendent jusqu'à la limite du plateau suggère la présence de l'inlandsis à cet endroit. Ce type de linéation profilée, subparallèle et très allongée est une signature irrévocable de l'activité des courants glaciaires et aurait servi de couloirs d'alimentation aux systèmes d'EGs. Les sédiments ont probablement été transportés sous la forme de coulées de débris et de turbidites durant le dernier épisode glaciaire par plusieurs petits canyons et ravins pour finalement s'accumuler au bas de la pente continentale sous la forme d'éventails glaciogéniques.

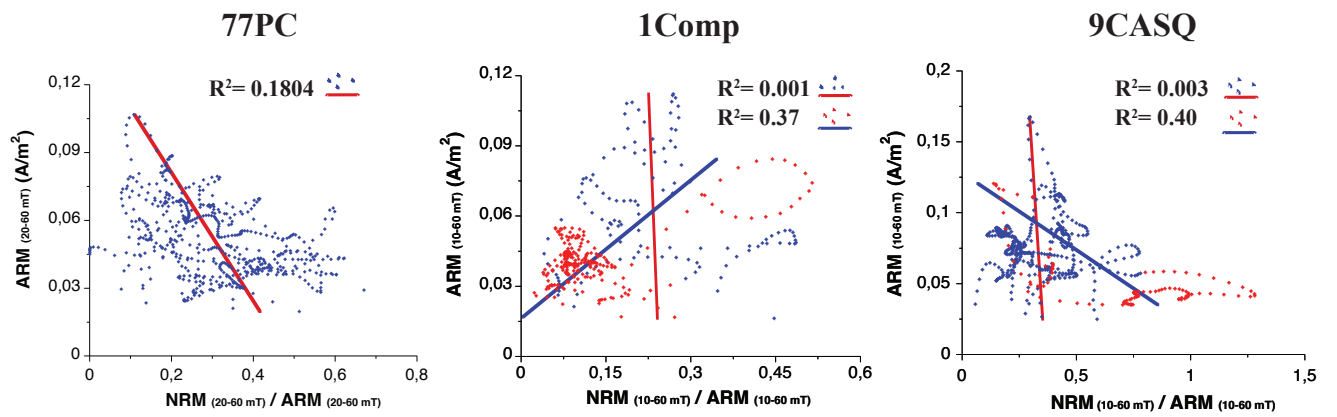
Ces reliefs sous-marins révèlent une épaisse couche de glace dynamique, des flux de glace et un écoulement sous-glaciaire qui suggèrent la présence d'une marge glaciaire de vêlage sur le plateau. Ces résultats, jumelé avec la datation des coulées de débris glaciogéniques et des turbidites démontrent l'activité des processus glaciaires antérieurs à la limite du plateau continental et permettent de définir une nouvelle extension maximale de l'IL dans le centre-ouest de la baie de Baffin durant le dernier épisode glaciaire. Afin d'appuyer

cette hypothèse, de nouvelles carottes sédimentaires devraient être prélevées à l'intérieur des éventails glaciogéniques adjacents à ceux où ont été prélevés les carottes AMD16-LGM-09 et AMD0217-01 afin d'identifier et de dater des turbidites et des coulées de débris glaciogénique. Une nouvelle campagne sismique plus en amont, dans la région de Home Bay, pourrait également venir délimiter avec précision les MSGs laissés par le passage de l'inlandsis dans cette région. En terminant, cette étude illustre clairement l'intérêt de combiner des âges radiocarbone avec des analyses paléomagnétiques pour établir le cadre chronostratigraphique dans les régions touchées par une importante dissolution des carbonates.

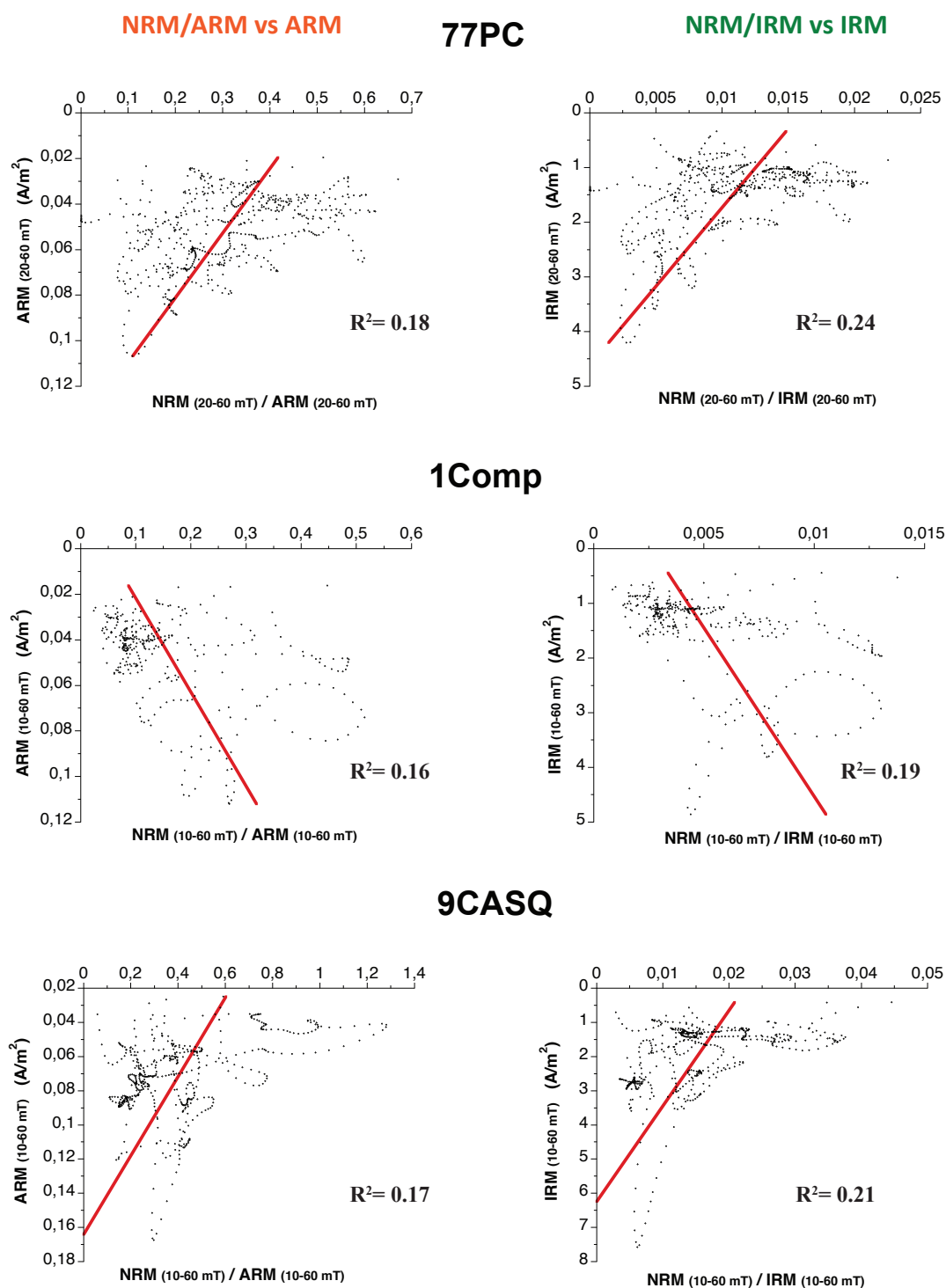


## ANNEXE I

### MATÉRIEL SUPPLÉMENTAIRE

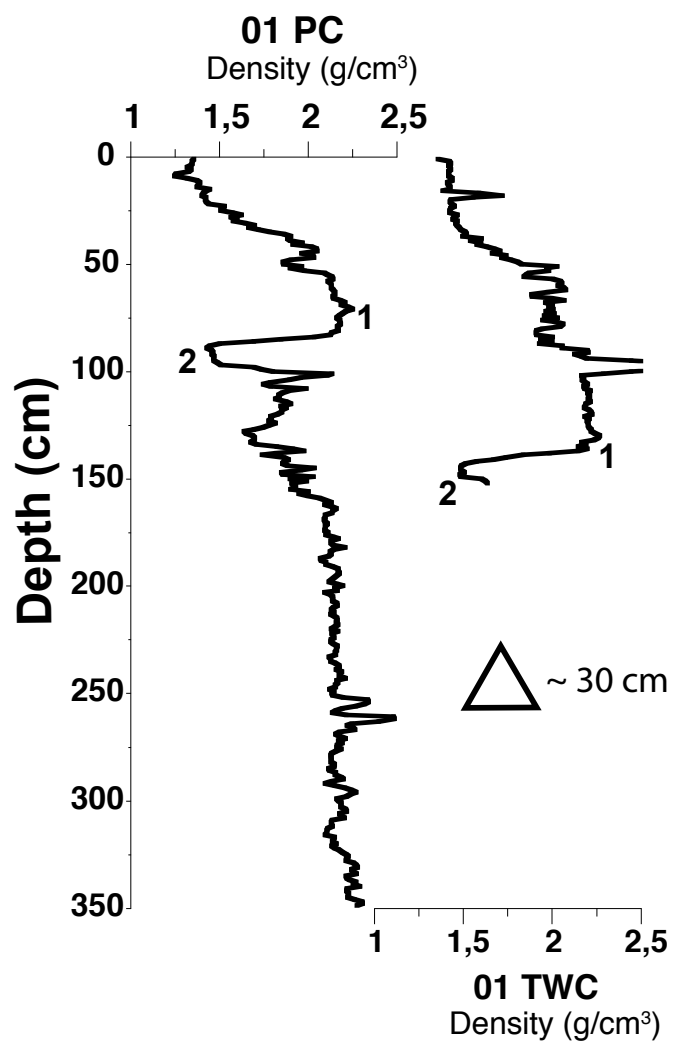


**Figure S1 :** RPI proxy vs. its normalizer for cores 77PC, 1Comp and 9CASQ : RDLs = red points and blue line ; REMAINING SEDIMENT = blue points and red line

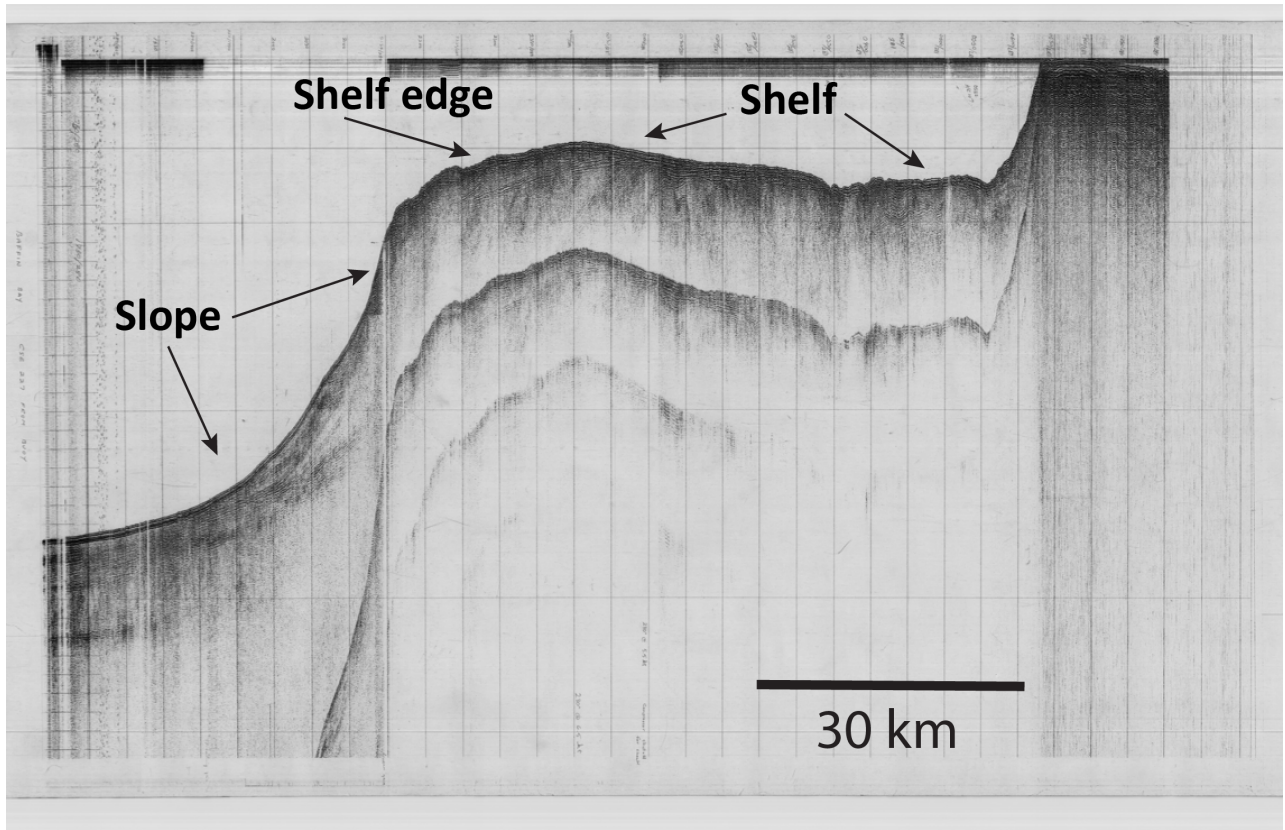


**Figure S2 :** RPI proxy vs. its normalizer ARM and IRM for cores 77PC, 1Comp and 9CASQ





**Figure S3 :** Correlation of cores 01-PC and 01-TWC (AMD0217-01 => 1Comp) based on density. Open delta symbol represents the difference between each core. The numbers represent tie-points between the two cores.



**Figure S4 :** Line 76029\_AG\_280\_1730 (airgun profile) collected in 1976 on board the CCGS Hudson by the Geological Survey of Canada. This figure do not show any grounding-zone wedge (GZW) in the sector.

## CHAPITRE 2

### RÉFÉRENCES BIBLIOGRAPHIQUES

Aksu, A.E., Piper, D.J.W., 1987. Late Quaternary sedimentation in Baffin Bay. *Can. J. Earth Sci.* 24, 1833–1846.

Andrews, J. et al., 1998. Late Quaternary stratigraphy, chronology, and depositional processes on the slope of SE Baffin Island, detrital carbonate and Heinrich events : Implications for onshore glacial history. *Géographie physique et Quaternaire*, 52(1), pp.91–105.

Andrews, J.T., 1990. Fiord to Deep Sea Sediment Transfers Along the North-Eastern Canadian Continental Margin : Models and Data. *Geogr. Phys. Quat.* 44, 55–70. doi :10.7202/032798ar

Andrews, J.T. et al., 2009. Late Quaternary stratigraphy, chronology, and depositional processes on the slope of S.E. Baffin Island, detrital carbonate and Heinrich events : Implications for onshore glacial history. *Géographie physique et Quaternaire*, 52, pp.91–105.

Andrews, J.T. et al., 1991. The surficial geology of the Canadian eastern Arctic and Polar continental shelves. *Continental Shelf Research*, 11(8–10), pp.791–819.

Andrews, J.T., Jennings, A.E., 1990. Geomagnetic Secular Variations (Inclination) of High-Latitude Fjord Cores - Eastern Canadian Arctic. *Polar Res.* 8, 245–259. doi :10.1111/j.1751-8369.1990.tb00387.x

Balkwill, H.R., McMillan, N.J., MacLean, B., 1990. Geology of the Labrador Shelf, Baffin Bay, and Davis Strait : in *Geology of the Continental Margin of Eastern Canada*, Keen, MJ and Williams, GL (Eds.), *The Geology of North America*, Vol. I-1. *Geol. Sur. Can* 295–348.

Balsam, W.L., Deaton, B.C., Damuth, J.E., 1999. Evaluating optical lightness as a

proxy for carbonate content in marine sediment cores. *Mar. Geol.* 161, 141–153.

Barletta, F., St-Onge, G., Channell, J.E.T., Rochon, A., 2010. Dating of Holocene western Canadian Arctic sediments by matching paleomagnetic secular variation to a geomagnetic field model. *Quat. Sci. Rev.* 29, 2315–2324. doi :10.1016/j.quascirev.2010.05.035

Barletta, F., St-Onge, G., Channell, J.E.T., Rochon, A., Polyak, L., Darby, D., 2008. High-resolution paleomagnetic secular variation and relative paleointensity records from the western Canadian Arctic : implication for Holocene stratigraphy and geomagnetic field behaviour. *Can. J. Earth Sci.* 45, 1265–1281. doi :10.1139/E08-039

Batchelor, C.L. and Dowdeswell, J.A., 2015. Ice-sheet grounding-zone wedges (GZWs) on high-latitude continental margins. *Marine Geology*, 363, pp.65–92. Available at : <http://dx.doi.org/10.1016/j.margeo.2015.05.001>.

De Blasio, F. V. et al., 2004. Flow models of natural debris flows originating from overconsolidated clay materials. *Marine Geology*, 213(1–4), pp.439–455.

De Blasio, F. V et al., 2006. Understanding the high mobility of subaqueous debris flows. *Norwegian Journal of Geology*, 86, pp.275–284.

Bourget, J. et al., 2011. Turbidite system architecture and sedimentary processes along topographically complex slopes : the Makran convergent margin. *Sedimentology*, 58(2), pp.376–406.

Briner, J.P., Michelutti, N., Francis, D.R., Miller, G.H., Axford, Y., Wooller, M.J., Wolfe, A.P., 2006. A multi-proxy lacustrine record of Holocene climate change on northeastern Baffin Island, Arctic Canada. *Quat. Res.* 65, 431–442.

Brouard, E., Lajeunesse, P., 2017. Maximum extent and decay of the Laurentide Ice Sheet in Western Baffin Bay during the Last glacial episode. *Sci. Rep.* 1–8. doi :10.1038/s41598-017-11010-9

Campbell, D.C., 2014. CCGS Hudson Expedition 2013-029. Geological Hazard As-

assessment of Baffin Bay and Biodiversity Assessment of Hatton Basin.

Campbell, D.C., Bennett, J.R., 2014. Preliminary results from recent investigations of marine geological hazards in Baffin Bay, Nunavut and Greenland. *Summ. Act.* 121–128.

Carter, R.M., Carter, L. and McCave, I.N., 1996. Current controlled sediment deposition from the shelf to the deep ocean : the Cenozoic evolution of circulation through the SW Pacific gateway. *Geologische Rundschau*, 85(3), pp.438–451.

Channell, J.E.T., Hodell, D.A., Romero, O., Hillaire-Marcel, C., De Vernal, A., Stoner, J.S., Mazaud, A., Röhl, U., 2012. A 750-kyr detrital-layer stratigraphy for the North Atlantic (IODP Sites U1302–U1303, Orphan Knoll, Labrador Sea). *Earth Planet. Sci. Lett.* 317, 218–230.

Clark, C.D., Tulaczyk, S.M., Stokes, C.R., Canals, M., 2003. A groove-ploughing theory for the production of mega-scale glacial lineations, and implications for ice-stream mechanics. *J. Glaciol.* 49, 240–256.

Coulthard, R.D., Furze, M.F.A., Pieńkowski, A.J., Nixon, F.C., England, J.H., 2010. New marine  $\Delta R$  values for Arctic Canada. *Quat. Geochronol.* 5, 419–434.

Cowan, E.A., Cai, J., Powell, R.D., Clark, J.D., Pitcher, J.N., 1997. Temperate glacial-marine varves : an example from Disenchantment Bay, southern Alaska. *J. Sediment. Res.* 67.

Cowan, E.A., Powell, R.D., 1990. Suspended sediment transport and deposition of cyclically interlaminated sediment in a temperate glacial fjord, Alaska, USA. *Geol. Soc. London, Spec. Publ.* 53, 75–89.

Day, R., Fuller, M., Schmidt, V.A., 1977. Hysteresis properties of titanomagnetites : grain-size and compositional dependence. *Phys. Earth Planet. Inter.* 13, 260–267.

De Vernal, A., Bilodeau, G., Hillaire-Marcel, C., Kassou, N., 1992. Quantitative assess-

ment of carbonate dissolution in marine sediments from foraminifer linings vs. shell ratios : Davis Strait, northwest North Atlantic. *Geology* 20, 527–530.

De Vernal, A., Hillaire-Marcel, C., Aksu, A.E., Mudie, P.J., 1987. Palynostratigraphy and chronostratigraphy of Baffin Bay deep sea cores : climatostratigraphic implications. *Palaeogeogr. Palaeoclimatol. Palaeoecol.* 61, 97–105.

Domack, E.W., 1990. Laminated terrigenous sediments from the Antarctic Peninsula : the role of subglacial and marine processes. *Geol. Soc. London, Spec. Publ.* 53, 91–103.

Dowdeswell, J.A., Canals, M., Jakobsson, M., Todd, B.J., Dowdeswell, E.K., Hogan, K.A., 2016. *Atlas of Submarine Glacial Landforms*.

Dowdeswell, J.A., Cofaigh, C.Ó., Noormets, R., Larter, R.D., Hillenbrand, C.-D., Bennetti, S., Evans, J., Pudsey, C.J., 2008. A major trough-mouth fan on the continental margin of the Bellingshausen Sea, West Antarctica : the Belgica Fan. *Mar. Geol.* 252, 129–140.

Dowdeswell, J.A., Cromack, M., 1991. Behavior of a glacier-derived suspended sediment plume in a small Arctic inlet. *J. Geol.* 99, 111–123.

Dowdeswell, J.A., Elverhfi, A., Spielhagen, R., 1998. Glacimarine sedimentary processes and facies on the polar North Atlantic margins. *Quat. Sci. Rev.* 17, 243–272.

Dowdeswell, J.A., Ottesen, D., 2013. Buried iceberg ploughmarks in the early Quaternary sediments of the central North Sea : a two-million year record of glacial influence from 3D seismic data. *Mar. Geol.* 344, 1–9.

Dowdeswell, J.A., Villinger, H., Whittington, R.J., Marienfeld, P., 1993. Iceberg scouring in Scoresby Sund and on the East Greenland continental shelf. *Mar. Geol.* 111, 37–53.

Dowdeswell, J.A., Whittington, R.J., Jennings, A.E., Andrews, J.T., Mackensen, A., Marienfeld, P., 2000. An origin for laminated glacimarine sediments through sea-ice build-up and suppressed iceberg rafting. *Sedimentology* 47, 557–576. doi :10.1046/j.1365-3091.2000.00306.x

Dunlap, E. and Tang, C.C.L., 2006. Modelling the mean circulation of Baffin Bay. *Atmosphere-Ocean*, 44(1), pp.99–109.

Dyke, A.S., Prest, V.K., 1987. Late Wisconsinan and Holocene History of the Laurentide Ice Sheet. *Géographie Phys. Quat.* 41, 237.

Dyke, A.S. et al., 2002. The Laurentide and Innuitian ice sheets during the last glacial maximum. *Quaternary Science Reviews*, 21(1), pp.9–31.

Dyke, a S., 2004. An outline of the deglaciation of North America with emphasis on central and northern Canada. *Quat. Glaciat. Chronol. Part II North Am.* 2b, 373-424.

Funder, S., Kjeldsen, K.K., Kjær, K.H., Cofaigh, C.Ó., 2011. The Greenland Ice Sheet during the past 300,000 years : A review, in : *Developments in Quaternary Sciences*. Elsevier, pp. 699–713.

Harrison, J.C., St-Onge, M.R., Petrov, O., Strelnikov, S., Lopatin, B., Wilson, F., Tella, S., Paul, D., Lynds, T., Shokalsky, S., 2008. Geological map of the Arctic. Geological Survey of Canada. Open File 5816.

Hesse, R. et al., 1997. Asymmetrical turbid surface-plume deposition near ice-outlets of the Pleistocene Laurentide ice sheet in the Labrador Sea. *Geo-Marine Letters*, 17(3), pp.179–187.

Hesse, R., Klauck, I., Khodabakhsh, S., Piper, D., 1999. Continental slope sedimentation adjacent to an ice margin. III. The upper Labrador Slope. *Mar. Geol.* 155, 249–276.

Hiscott, R.N. and Aksu, A.E., 1994. Submarine debris flows and continental slope evolution in front of Quaternary ice sheets, Baffin Bay, Canadian Arctic. *AAPG bulletin*, 78(3), pp.445–460.

Hiscott, R.N., Aksu, A.E. and Nielsen, O.B., 1989. Provenance and dispersal patterns, Pliocene-Pleistocene section at site 645, Baffin Bay. In *Proc. Ocean Drill. Program Sci. Re-*

sults. pp. 31–52.

Hodell, D.A., Channell, J.E.T., Curtis, J.H., Romero, O.E., Röhl, U., 2008. Onset of “Hudson Strait” Heinrich events in the eastern North Atlantic at the end of the middle Pleistocene transition ( $\sim 640$  ka)? *Paleoceanography* 23.

Hoffman, P.F., Bally, A.W. and Palmer, A.R., 1989. Precambrian geology and tectonic history of North America. *The geology of North America—an overview*, pp.447–512.

Hollister, C.D., 1967. Sediment distribution and deep circulation in the western North Atlantic, Thesis (Ph. D.)-Columbia University.

Hollister, C.D. and Heezen, B.C., 1972. Geological effects of ocean bottom currents. *Studies in Physical Oceanography : A Tribute to George Wust on his 80th Birthday*, 2, pp.37–66.

Jackson, R., Carlson, A.E., Hillaire-Marcel, C., Wacker, L., Vogt, C., Kucera, M., 2017. Asynchronous instability of the North American-Arctic and Greenland ice sheets during the last deglaciation. *Quat. Sci. Rev.* 164, 140–153.

Jakobsson, M. et al., 2012. The international bathymetric chart of the Arctic Ocean (IBCAO) version 3.0. *Geophysical Research Letters*, 39(12).

Jenner, K.A., Campbell, D.C., Piper, D.J.W., 2018. Along-slope variations in sediment lithofacies and depositional processes since the Last Glacial Maximum on the northeast Baffin margin, Canada. *Mar. Geol.* pagerange. doi :<https://doi.org/10.1016/j.margeo.2018.07.012>

Jennings, A., 1993. The Quaternary history of Cumberland Sound, southeastern Baffin Island : the marine evidence. *Géographie Phys. Quat.* 47, 21–42.

King, E.L., Haflidason, H., Sejrup, H.P., 1998. Glacigenic debris flows on the North Sea Trough Mouth Fan during ice stream maxima. *Mar. Geol.* 152, 217–246.

King, J.W., Banerjee, S.K., Marvin, J., 1983. A new rock-magnetic approach to selec-



ting sediments for geomagnetic paleointensity studies : Application to paleointensity for the last 4000 years. *J. Geophys. Res. Solid Earth* 88, 5911-5921.

Kissel, C., Mazaud, A., Channell, J.E.T., Beer, J., 2000. North Atlantic palaeointensity stack since 75ka (NAPIS-75) and the duration of the Laschamp event. *Philos. Trans. R. Soc. London A Math. Phys. Eng. Sci.* 358, 1009–1025.

Laberg, J.S. and Vorren, T.O., 1993. A late Pleistocene submarine slide on the Bear Island trough mouth fan. *Geo-Marine Letters*, 13(4), pp.227–234.

Laberg, J.S., Vorren, T.O., 1995. Late Weichselian submarine debris flow deposits on the Bear Island Trough Mouth Fan. *Mar. Geol.* 127, 45–72. doi :10.1016/0025-3227(95)00055-4

Laj, C., Kissel, C., Mazaud, A., Channell, J.E.T., Beer, J., 2000. North Atlantic Paleointensity Stack since 75 ks (NAPIS-75) and the duration of the Laschamp event, *Philos. Transact. Ser. A Math Phys. Eng. Sci.* 358, 1009–1025.

Lasabuda, A. et al., 2018. Late Cenozoic erosion estimates for the northern Barents Sea : Quantifying glacial sediment input to the Arctic Ocean. *Geochemistry, Geophysics, Geosystems*.

Ledu, D., Rochon, A., de Vernal, A., St-Onge, G., 2008. Palynological evidence of Holocene climate change in the eastern Arctic : a possible shift in the Arctic oscillation at the millennial time scale. *Can. J. Earth Sci.* 45, 1363–1375.

Levi, S., Banerjee, S.K., 1976. On the possibility of obtaining relative paleointensities from lake sediments. *Earth Planet. Sci. Lett.* 29, 219–226.

Li, G., Piper, D.J.W., Campbell, D.C., Mosher, D., 2012. Turbidite deposition and the development of canyons through time on an intermittently glaciated continental margin : The Bonanza Canyon system, offshore eastern Canada. *Mar. Pet. Geol.* 29, 90–103.

Li, G., Piper, D.J.W., Calvin Campbell, D., 2011. The Quaternary Lancaster Sound trough mouth fan, NW Baffin Bay. *Journal of Quaternary Science*, 26(5), pp. 511 – 522.

Lisé-Pronovost, A., St-Onge, G., Brachfeld, S., Barletta, F., Darby, D., 2009. Paleomagnetic constraints on the Holocene stratigraphy of the Arctic Alaskan margin. *Glob. Planet. Change* 68, 85–99. doi :10.1016

Lovell, J.P.B. and Stow, D.A. V, 1981. Identification of ancient sandy contourites. *Geology*, 9(8), pp.347–349.

Lucchi, R.G. et al., 2013. Postglacial sedimentary processes on the Storfjorden and Kveithola trough mouth fans : Significance of extreme glacialmarine sedimentation. *Global and planetary change*, 111, pp.309–326.

Margold et al., 2015. Ice streams in the Laurentide Ice Sheet : a new mapping inventory. *Journal of Maps*, 11(3), pp.380–395.

Margold, Stokes, C.R., Clark, C.D., Kleman, J., 2015. Ice streams in the Laurentide Ice Sheet : a new mapping inventory. *J. Maps* 11, 380–395. doi :10.1080/17445647.2014.912036

Mazaud, A., 2005. User-friendly software for vector analysis of the magnetization of long sediment cores. *Geochemistry, Geophys. Geosystems* 6.

McCann, S.B., 1988. Quaternary environments : Eastern Canadian Arctic, Baffin Bay and Western Greenland, JT Andrews (Ed.), Allen and Unwin, Boston, 1985. No. of pages : 774. ISBN 0 04 551094 6. *Earth Surf. Process. Landforms* 13, 92–94.

McKay, J.L., de Vernal, A., Hillaire-Marcel, C., Not, C., Polyak, L., Darby, D., 2008. Holocene fluctuations in Arctic sea-ice cover : dinocyst-based reconstructions for the eastern Chukchi Sea. *Can. J. Earth Sci.* 45, 1377–1397.

Meynadier, L., Valet, J.-P., Weeks, R., Shackleton, N.J., Hagee, V.L., 1992. Relative geomagnetic intensity of the field during the last 140 ka. *Earth Planet. Sci. Lett.* 114, 39–57.

Montelli, A., Dowdeswell, J.A., Ottesen, D., Johansen, S.E., 2017. Ice-sheet dynamics through the Quaternary on the mid-Norwegian continental margin inferred from 3D seismic data. *Mar. Pet. Geol.* 80, 228–242. doi :10.1016/j.marpetgeo.2016.12.002

Mutti, M. dei S.E., 1977. Distinctive thin-bedded turbidite facies and related depositional environments in the Eocene Hecho Group (South-central Pyrenees, Spain). *Sedimentology* 24, 107-131.

Nemec, W., 1990. Aspects of sediment movement on steep delta slopes. In *Coarse-grained deltas*. pp. 29–73.

Nygard, A., Sejrup, H.P., Haflidason, H., King, E.L., 2002. Geometry and genesis of glacial debris flows on the North Sea Fan : TOBI imagery and deep-tow boomer evidence. *Mar. Geol.* 188, 15-33. doi :10.1016/S0025-3227(02)00273-6

Ó Cofaigh, C., Andrews, J.T., Jennings, A.E., Dowdeswell, J.A., Hogan, K.A., Kilfeather, A.A., Sheldon, C., 2013. Glacimarine lithofacies, provenance and depositional processes on a West Greenland trough-mouth fan. *J. Quat. Sci.* 28, 13-26.

Ó Cofaigh, C., Taylor, J., Dowdeswell, J.A., Pudsey, C.J., 2003. Palaeo-ice streams, trough mouth fans and high-latitude continental slope sedimentation. *Boreas* 32, 37–55. doi :Doi 10.1080/03009480310001858

Ottesen, D., Dowdeswell, J.A., Rise, L., 2005. Submarine landforms and the reconstruction of fast-flowing ice streams within a large Quaternary ice sheet : the 2500-km-long Norwegian-Svalbard margin (57–80 N). *Geol. Soc. Am. Bull.* 117, 1033–1050.

Philippe, É.G.H. et al., Are Paleomagnetic Records From U[+2010] Channels Appropriate for Studies of Reversals and Excursions ? *Geochemistry, Geophysics, Geosystems*.

Piper, D.J.W., 1972. Sediments of the Middle Cambrian Burgess Shale, Canada. *Lethaia*, 5(2), pp.169–175.

Piper, D.J.W., Normark, W.R., 2009. Processes that initiate turbidity currents and their influence on turbidites : a marine geology perspective. *J. Sediment. Res.* 79, 347–362.

Pouderoux, H. et al., 2012. Postglacial (after 18 ka) deep-sea sedimentation along the Hikurangi subduction margin (New Zealand) : Characterisation, timing and origin of turbidites. *Marine Geology*, 295, pp.51–76.

Praeg, D.B., MacLean, B. and Sonnichsen, G. V, 2006. Quaternary geology of the northeast Baffin Island continental shelf, Cape Aston to Buchan Gulf (70° to 72° N), Geological Survey of Canada.

Rebesco, M., Hernández-Molina, F.J., Van Rooij, D., Wåhlin, A., 2014. Contourites and associated sediments controlled by deep-water circulation processes : state-of-the-art and future considerations. *Mar. Geol.* 352, 111–154.

Reimer, P.J., Bard, E., Bayliss, A., Beck, J.W., Blackwell, P.G., Ramsey, C.B., Buck, C.E., Cheng, H., Edwards, R.L., Friedrich, M., 2013. IntCal13 and Marine13 radiocarbon age calibration curves 0–50,000 years cal BP. *Radiocarbon* 55, 1869–1887.

Roger, J., Saint-Ange, F., 2013. Late Quaternary glacial history and meltwater discharges along the Northeastern Newfoundland Shelf. *Can. J. Earth Sci.* 1194, 1178–1194. doi :[dx.doi.org/10.1139/cjes-2013-0096](https://doi.org/10.1139/cjes-2013-0096)

Scotese, C.R. and Golonka, J., 1997. Paleogeographic atlas, PALEOMAP Project, University of Texas at Arlington.

Shanmugam, G., 2006. Deep-water processes and facies models : Implications for sandstone petroleum reservoirs, Elsevier.

Simon, Q., St-Onge, G., Hillaire-Marcel, C., 2012a. Late Quaternary chronostratigraphic framework of deep Baffin Bay glaciomarine sediments from high-resolution paleomagnetic data. *Geochemistry, Geophys. Geosystems* 13, 1–24. doi :[10.1029/2012GC004272](https://doi.org/10.1029/2012GC004272)

Simon, Q., St-Onge, G., Hillaire-Marcel, C., 2013. Propriétés magnétiques, minéralogiques et sédimentologiques des sédiments profonds de la baie de Baffin : chronologie et dynamique des glaciers ouest groenlandais, innuitiens et laurentidiens au cours de la dernière glaciation.

Simon, Q., St-Onge, G., Hillaire-Marcel, C., 2012b. Detrital carbonate events in Baffin bay during the last climatic cycle : their timing vs. the Greenland Dansgaard-Oeschger cycles and north Atlantic Heinrich events, in : 2012 GSA Annual Meeting in Charlotte.

Snowball, I., Muscheler, R., 2007. Palaeomagnetic intensity data : an Achilles heel of solar activity reconstructions. *The Holocene* 17, 851–859. doi :10.1177/0959683607080531

Snowball, I., Sandgren, P., 2002. Geomagnetic field variations in northern Sweden during the Holocene quantified from varved lake sediments and their implications for cosmogenic nuclide production rates. *The Holocene* 12, 517–530. doi :10.1191/0959683602hl562rp

St-Onge, G. et al., 2007. Chapter two continuous physical properties of cored marine sediments. *Developments in marine geology*, 1, pp.63–98.

St-Onge, G. et al., 2004. Earthquake and flood-induced turbidites in the Saguenay Fjord (Québec) : A Holocene paleoseismicity record. *Quaternary Science Reviews*, 23(3–4), pp.283–294.

St-Onge, G. et al., 2008. Identification and dating of a key Late Pleistocene stratigraphic unit in the St. Lawrence Estuary and Gulf (Eastern Canada). *Quaternary Science Reviews*, 27(25–26), pp.2390–2400.

St-Onge, G. and Stoner, J.S., 2011. Paleomagnetism Near The North Magnetic Pole. *Oceanography*, 24(3), pp.162–173. Available at : <http://dx.doi.org/10.5670/oceanog.2011.80>.

St-Onge, G., Stoner, J.S. and Hillaire-Marcel, C., 2003. Holocene paleomagnetic records from the St. Lawrence Estuary, eastern Canada : Centennial- to millennial-scale geomagnetic modulation of cosmogenic isotopes. *Earth and Planetary Science Letters*, 209(1–2), pp.113–130.

Stanley, S, Luczaj, J.A., 2015. Earth system history, Fourth Edi. ed. Macmillan, New York

Stein, S. et al., 1979. Earthquakes along the passive margin of eastern Canada. *Geophysical Research Letters*, 6(7), pp.537–540.

Stokes, C.R., 2017a. Deglaciation of the Laurentide Ice Sheet from the Last Glacial Maximum. *J. Bus. ethics* 44, 0–103. doi :10.1063/1.2756072

Stokes, C.R., 2017b. Deglaciation of the Laurentide Ice Sheet from the Last Glacial Maximum. *Cuad. Investig. geográfica*. 43, 377–428.

Stokes, C.R., Clark, C.D., 2002. Are long subglacial bedforms indicative of fast ice flow ? *Boreas* 31, 239–249.

Stoner, J.S., Channell, J.E.T., Hillaire-Marcel, C., Kissel, C., 2000. Geomagnetic paleointensity and environmental record from Labrador Sea core MD95-2024 : Global marine sediment and ice core chronostratigraphy for the last 110 kyr. *Earth Planet. Sci. Lett.* 183, 161–177. doi :10.1016/S0012-821X(00)00272-7

Stoner, J.S., Jennings, A., Kristjánsdóttir, G.B., Dunhill, G., Andrews, J.T., Hardardóttir, J., 2007. A paleomagnetic approach toward refining Holocene radiocarbon-based chronologies : Paleoceanographic records from the north Iceland (MD99-2269) and east Greenland (MD99-2322) margins. *Paleoceanography* 22, 1–23. doi :10.1029/2006PA001285

Stoner, J.S., St-Onge, G., 2007. Chapter Three Magnetic Stratigraphy in Paleoceanography : Reversals, Excursions, Paleointensity, and Secular Variation. *Dev. Mar. Geol.* 1, 99–138. doi :10.1016/S1572-5480(07)01008-1

Stow, D.A. V and Piper, D.J.W., 1984. Deep-water fine-grained sediments : facies models. Geological Society, London, Special Publications, 15(1), pp.611–646.

Stuiver, M., Reimer, P.J., 1993. Extended 14 C data base and revised CALIB 3.0 14 C

age calibration program. *Radiocarbon* 35, 215–230.

Syvitski, J.P.M., 1989. On the deposition of sediment within glacier-influenced fjords : oceanographic controls. *Mar. Geol.* 85, 301–329.

Talling, P.J., 2014. On the triggers, resulting flow types and frequencies of subaqueous sediment density flows in different settings. *Mar. Geol.* 352, 155–182. doi :10.1016/j.margeo.2014.02.006

Talling, P.J. et al., 2007. Onset of submarine debris flow deposition far from original giant landslide. *Nature*, 450(7169), pp.541–544.

Talling, P.J., Paull, C.K., Piper, D.J.W., 2013. How are subaqueous sediment density flows triggered, what is their internal structure and how does it evolve ? Direct observations from monitoring of active flows. *Earth-Science Rev.* 125, 244–287. doi :10.1016/j.earscirev.2013.07.005

Tang, C.C.L., Ross, C.K., Yao, T., Petrie, B., DeTracey, B.M., Dunlap, E., 2004. The circulation, water masses and sea-ice of Baffin Bay. *Prog. Oceanogr.* 63, 183–228.

Tanty, C. et al., 2016. Acquisition of detrital magnetization in four turbidites. *Geochemistry, Geophysics, Geosystems*, 17(8), pp.3207–3223.

Tauxe, L., 2010. *Essentials of paleomagnetism*. Univ of California Press.

Tauxe, L., 1993. Sedimentary records of relative paleointensity of the geomagnetic field : theory and practice. *Rev. Geophys.* 31, 319–354.

Tauxe, L., Wu, G., 1990. Normalized remanence in sediments of the western equatorial Pacific : relative paleointensity of the geomagnetic field ? *J. Geophys. Res. Solid Earth* 95, 12337–12350.

Taylor, J., Dowdeswell, J.A., Kenyon, N.H., Cofaigh, C.Ó., 2002. Late Quaternary architecture of trough-mouth fans : debris flows and suspended sediments on the Norwegian margin. *Geol. Soc. London, Spec. Publ.* 203, 55–71.

Toucanne, S., Zaragosi, S., Bourillet, J.F., Dennielou, B., Jorry, S.J., Jouet, G., Cremer, M., 2012. External controls on turbidite sedimentation on the glacially-influenced Armorican margin (Bay of Biscay, western European margin). *Mar. Geol.* 303–306, 137–153. doi :10.1016/j.margeo.2012.02.008

Tripsanas, E.K., Piper, D.J.W., 2008. Late Quaternary stratigraphy and sedimentology of Orphan Basin : implications for meltwater dispersal in the southern Labrador Sea. *Palaeogeogr. Palaeoclimatol. Palaeoecol.* 260, 521–539.

Vorren, T.O., Laberg, J.S., Blaume, F., Dowdeswell, J.A., Kenyon, N.H., Mienert, J., Rumohr, J.A.N., Werner, F., 1998. The Norwegian–Greenland Sea continental margins : morphology and late Quaternary sedimentary processes and environment. *Quat. Sci. Rev.* 17, 273–302.

Winsor, K., Carlson, A.E., Klinkhammer, G.P., Stoner, J.S., Hatfield, R.G., 2012. Evolution of the northeast Labrador Sea during the last interglaciation. *Geochemistry, Geophys. Geosystems* 13.

Wynn, R.B. and Stow, D.A. V, 2002. Classification and characterisation of deep-water sediment waves. *Marine Geology*, 192(1–3), pp.7–22.

Yamazaki, T., Yamamoto, Y., Acton, G., Guidry, E.P., Richter, C., 2013. Rockmagnetic artifacts on longterm relative paleointensity variations in sediments. *Geochemistry, Geophys. Geosystems* 14, 29-43.